THESIS FOR THE DEGREE OF DOCTOR OF PHILOSOPHY

# Chemical Modification of Electrospun Cellulose Nanofibers

JOHANNES THUNBERG

*Department of Chemistry and Chemical Engineering*
CHALMERS UNIVERSITY OF TECHNOLOGY
Göteborg, Sweden 2015

**Chemical Modification of Electrospun Cellulose Nanofibers**
Johannes Thunberg

Göteborg 2015
ISBN: 978-91-7597-222-0



*Doktorsavhandlingar vid Chalmers tekniska högskola*
ISSN 0346-718X
löpnummer: 3903

Department of Chemistry and Chemical Engineering
CHALMERS UNIVERSITY OF TECHNOLOGY
SE-412 96 GÖTEBORG, Sweden
Phone: +46 (0)31-772 10 00

Cover: Functionalized electrospun cellulose, (left) MOF and (right) polypyrrole.

Printed by Chalmers Reproservice
Göteborg, Sweden 2015

# ABSTRACT

The forest industry is a large part of the Swedish economy and the export of pulp, paper and wood products constitutes 11% of the total Swedish export of goods. The main product of a pulp mill is purified cellulose, which has many great properties like biodegradability and non-toxicity. Cellulose pulps are mainly used for paper and board products whereas speciality pulp such as dissolving pulp is used for regenerated cellulose in fiber and cellophane production. Cellulose is difficult to dissolve and process, but some ionic liquids have the ability to dissolve cellulose. Ionic liquids also have low vapor pressure and low flammability which make them suitable for large scale processes.

In this thesis sub-micron scale cellulose nanofibers were created by electrospinning of cellulose from ionic liquid. Solution properties were studied and correlated to nanofiber formation. It was found that co-solvents could decrease viscosity and surface tension. As a consequence the rheological properties of the electrospun cellulose solutions could be linked to fiber formation. Successfully electrospun solutions had a high zero shear viscosity were highly shear thinning.

Electrospun cellulose nanofibers were thereafter further functionalized towards different applications. They were made conductive by synthesis of a polypyrrole layer on the nanofiber surface. It was shown that polypyrrole adhered to the nanofiber surface and increased the surface roughness of the nanofibers. The non-toxic property of cellulose was retained after polypyrrole synthesis and neural cell culture experiment indicated that polypyrrole enhanced cell adhesion to the nanofibers.

Electrospun cellulose nanofibers were chemically modified to give carboxylate rich surfaces. These anionic fibers were used as templates for synthesis of nano-porous structures of metal-organic framework (MOF). Carboxymethylated nanofibers had an even distribution of MOFs over the nanofiber surface. The MOF functionalized cellulose nanofibers had good adsorption properties and the surface area was greatly increased.

The concept of synthesizing MOFs on cellulose was transferred to another type of nano structured cellulose, cellulose nanofibrils (CNF), which currently can be produced in larger amounts than electrospun cellulose. A zeolitic imidazolate framework (ZIF) was synthesized on CNF in aqueous medium. Highly porous novel ZIF/CNF hybrid materials were created.



**Keywords:** Electrospinning, Cellulose, Nanocellulose, Ionic liquid, Cellulose Dissolution, Polypyrrole, Metal-organic Framework, Zeolitic Imidazolate Framework

LIST OF PUBLICATIONS

I **Electrospinning of cellulose nanofibers from ionic liquids: The effect of different cosolvents**
L. Härdelin, J. Thunberg, E. Perzon, G. Westman, P. Walkenström, P. Gatenholm
(2012), *J. Appl. Polym. Sci.*, 125 1901-1909.

II ***In Situ* Synthesis of Conductive Polypyrrole on Electrospun Cellulose Nanofibers: Scaffold for Neural Tissue Engineering**
J. Thunberg, T. Kalogeropoulos, V. Kuzmenko, D. Hägg, S. Johannesson, G. Westman and P. Gatenholm
(2015), *Cellulose*, 22 1459-1467.

III **Enhanced Synthesis of Metal-Organic Frameworks on the Surface of Electrospun Cellulose Nanofibers**
E. Laurila, J. Thunberg, S. P. Argent, N. R. Champness, S. Zacharias, G. Westman and L. Öhrström
(2015), *Adv. Eng. Mat.*, 17 1282-1286.

IV **Synthesis of Metal-Organic Frameworks on Nanocellulose in Aqueous Medium**
J. Thunberg, S. Zacharias, M. Hasani, L. Öhrström and G. Westman
*Manuscript*

Additional publications not included in this thesis

V **Enhanced growth of neural networks on conductive cellulose-derived nanofibrous scaffolds**
V. Kuzmenko, T. Kalogeropoulos, J. Thunberg, S. Johannesson, D. Hägg, P. Enoksson, P. Gatenholm
(2016), *Mater. Sci. Eng., C*, 58 14-23.

Part of this work has been presented by the author at:

**243rd ACS National Meeting and Exposition**,
25 – 29 Mars 2012, *San Diego, California*
Title: Effect of solvent on electrospun cellulose nanofiber

**EDANA Nonwovens Research Academy**[1],
19 – 20 April 2012, *Göteborg, Sweden*
Title: Dissolution of cellulose in ionic liquids

**241st ACS National Meeting and Exposition**,
27 – 31 Mars 2011, *Anaheim, California*
Title: Cellulose nanofibers electrospun from non volatile ionic liquid

**1st Avancell Conference**,
18 – 19 October 2011, *Göteborg, Sweden*
Title: Electrospinning of cellulose nanofibres from ionic liquids

**FPIRC Summer Conference**,
24 – 26 August 2010, *Karlstad, Sweden*
Title: Electrospun cellulose

[1] As part of site-visit to Chalmers University of Technology

CONTRIBUTION REPORT

I **Electrospinning of cellulose nanofibers from ionic liquids: The effect of different cosolvents**
Participated in the planning, prepared all solutions and performed electrospinning. Measured surface tension, conductivity and viscosity. Performed data analysis and contributed to the manuscript.

II **Enhanced Synthesis of Metal-Organic Frameworks on the Surface of Electrospun Cellulose Nanofibers**
Participated in the planning and performed the electrospinning. Performed the thermo gravimetric analysis and the scanning electron microscopy. Compiled data and wrote manuscript.

III ***In Situ* Synthesis of Conductive Polypyrrole on Electrospun Cellulose Nanofibers: Scaffold for Neural Tissue Engineering**
Participated in the planning and performed the electrospinning and polypyrrole synthesis. Performed the scanning electron microscopy and wrote manuscript.

IV **Synthesis of Metal-Organic Frameworks on Nanocellulose in Aqueous Medium**
Planned and performed experimental work. Wrote manuscript.

# Contents

# 1

# Introduction

## 1.1 Aim

The forest industry is a large part of the Swedish economy and has been so since the late $19^{\text{th}}$ century when the first Kraft pulp process was implemented. The export of pulp, paper and wood products constitutes 11% of the total Swedish export of goods[1]. The increase in Eucalyptus based forest industries around the world is a growing concern for the Swedish forest industry. The fast growing Eucalyptus tree requires less land areal than the slow growing Swedish Spruce and Pine. In addition, old forest products, such as newsprint, might be phased out in the near future

[1] According to the SCB Statistical database, the total Swedish export was 1 124 664 million SEK and wood and paper products were 124 176 million SEK in 2014

due to new technologies and changes in consumer patterns and lifestyles. There are different movements in Sweden to adapt to these changes. One such effort is the Wallenberg Wood Science Center (WWSC), funded by the Knut and Alice Wallenberg foundation. WWSC was created with the vision of becoming an internationally leading center for research within *new materials from trees*. Cellulose is one of the main constituents of wood and the objective of this work was to create new materials from electrospun cellulose.

- In Paper I, the aim was to explore new routes to efficient electrospinning of cellulose using ionic liquids, which is a new type of cellulose solvents with unique properties and cellulosic materials processed with ionic liquids are of high research interest. The study investigates how co-solvents together with ionic liquid can make the electrospinning process of cellulose more efficient and which solution properties are important in this type of electrospinning.
- In Paper II cellulose nanofibers were electrospun and chemically functionalized to give the resulting materials new properties. The nanofibers were made electrically conductive by *in situ* synthesis of a conductive polymer on the nanofiber surface. The nanofibers were then used as tissue engineering scaffolds.
- In Paper III, a copper based metal-organic framework (MOF) was *in situ* synthesized on cellulose nanofibers. Metal-organic frameworks are materials with high specific surface area, which are interesting for filtering or gas storage applications. Two different pretreatments of the cellulose surface were evaluated to improve adhesion between cellulose nanofibers and MOFs.
- In Paper IV, the concept of functionalizing cellulose with MOFs was taken to another type of fibrous cellulose material, cellulose nanofibrils. A Zinc based zeolitic imidazole framework was synthesized on cellulose nanofibrils. The aim of this work was to create a cellulose/MOF material without hazardous solvents, using water as reaction medium.

# 2

# Background

## 2.1 Cellulose in Wood

The outstanding properties of wood come from its function in the tree. A tree must be rigid but not stiff so it can bend in the wind without breaking. Wood must also be porous and have channels so that water can be transported through the stem, this porosity makes wood a relative light-weight material in the dry state. From a material point of view secondary cell wall of a softwood tracheid can be considered a three-dimensional fiber-reinforced composite. Strong linear cellulose fibrils give the load-bearing strength while lignin and hemicelluloses form an elastic matrix phase.

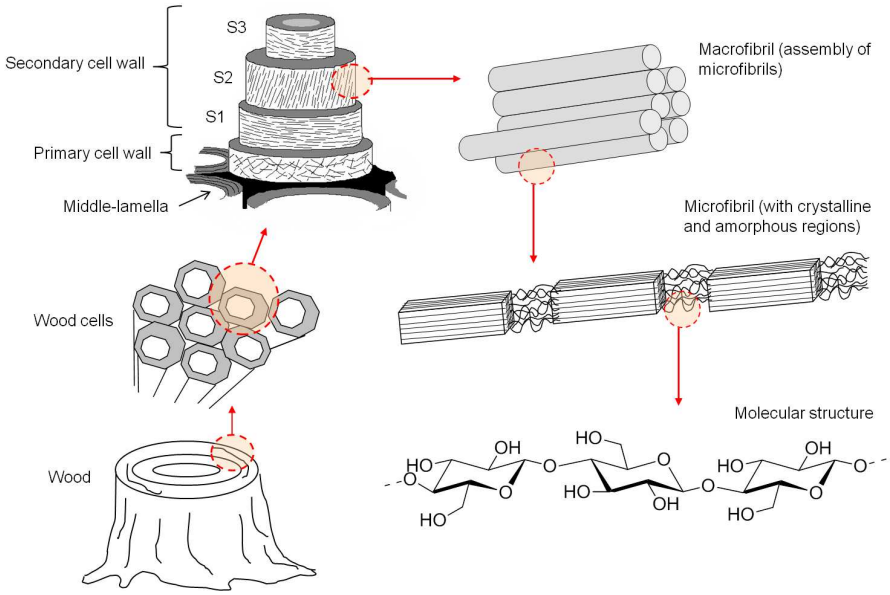


**Figure 2.1:** *Macroscopic to molecular structure of cellulose in wood (adapted from [Hasani, 2010], reprinted with permission).*

Wood has an anisotropic hierarchical structure, which is illustrated in Figure 2.1. On the macro-scale wood is composed mainly of elongated cells, called tracheids. These wood cells are mostly elongated in the stems longitudinal direction and are glued together by the middle lamella, a lignin rich layer. Cellulose is predominantly found inside the cell wall and the wood cell itself has a primary cell wall and a secondary cell wall. The cellulose microfibrils in the primary cell wall are randomly oriented, but ordered in the secondary cell wall, which contains three distinct layers, S1, S2 and S3. The thickest layer in the secondary cell wall is S2 and the microfibrils in this layer are mostly aligned in the fiber axis direction. The cellulose microfibrils themselves are built up of crystalline and amorphous regions as shown in Figure 2.1.

## 2.2 Molecular Structure of Cellulose

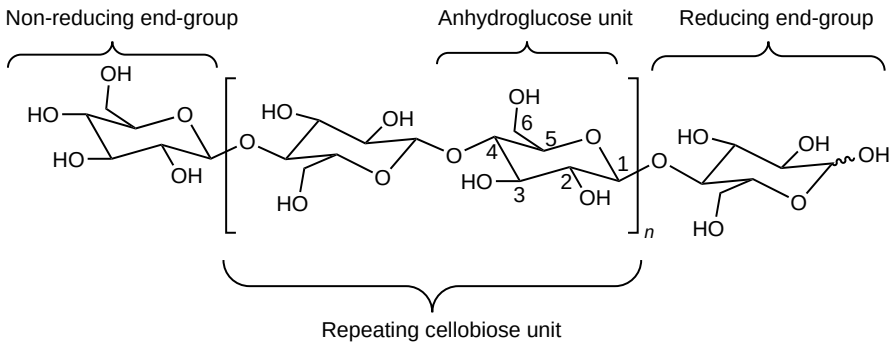


**Figure 2.2:** *Molecular structure of cellulose. The carbon atoms in the glucose ring are numbered according to established nomenclature. The glucose units are bonded by an ether linkage between carbon 1 and carbon 4. The oxygen of carbon 1 is in the $\beta$ position and this specific glycosidic bond is a called a $\beta$(1-4) linkage.*

In 1833 French agricultural scientist Anselme Payen studied starch and discovered the first enzyme diastase, which has the ability to break down starch to maltose. At that time the plant cell wall was thought to consist of a uniform substance specific to each species [Ott et al., 1954]. Payen extracted various plant tissues and a residue with the molecular formula $C_6H_{10}O_5$ persisted. The residue was a molecular isomer of starch and a main constituent of the plant cell wall, but it differed from starch in its properties. The residue was unresponsive to diastase but yielded glucose when degraded by acid. Starch turns blue with iodine but Payens newly found carbohydrate did not [Payen, 1838]. It was named cellulose in 1839 [Dumas et al., 1839]. The chemical structure of cellulose was unknown until the 1920s when methylation analysis made it clear that hydroxyl groups occupied the 2, 3 and 6 carbon [Irvine and Hirst, 1923]. These findings suggested that glucose in cellulose was linked together by the 1 and 4 carbon. The term macromolecule was coined by Hermann Staudinger in the 1920s and he suggested that cellulose along with many other natural polymers were long chains of covalently bonded repeating monomers [Staudinger, 1920; Staudinger and Fritschi, 1922]. Methylated end groups were isolated from the hy-

drolysis products of methylated cellulose in 1932 which gave the final proof that cellulose was a linear macromolecule [Haworth and Machemer, 1932]. The molec-

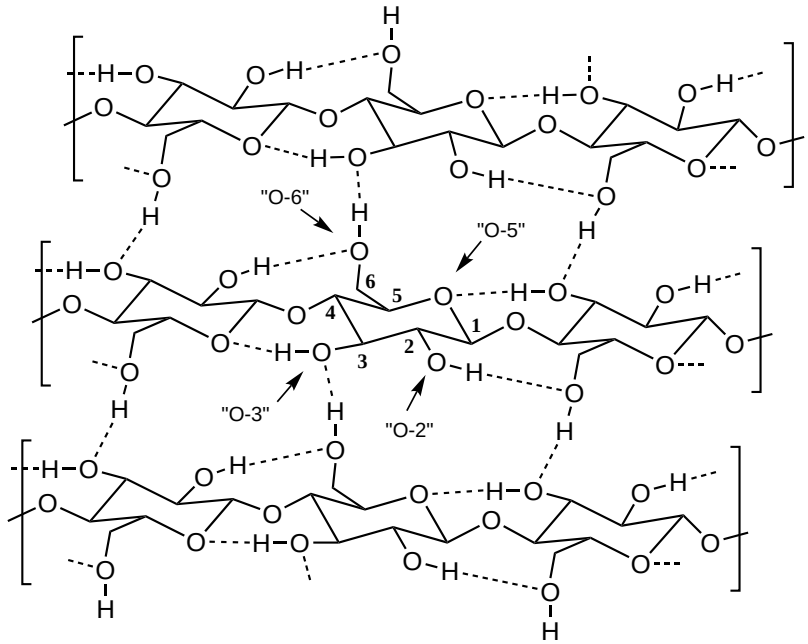


**Figure 2.3:** *Molecular model describing parallel polymer chain conformation in native cellulose. Dotted lines denote hydrogen bonding and numbers signify carbon number in AGU, according to the molecular structure in Figure 2.2.*

ular structure of cellulose is shown in Figure 2.2 and shows a linear polysaccharide of $\beta$(1-4) linked D-glucose units. The smallest monomer in the polymer chain is an Anhydrous Glucose Unit (AGU) and the repeating unit is a cellobiose unit. The glucose units are rotated 180° around the glycosidic bond. The reducing end-group is in equilibrium with its open ring formation containing an aldehyde group. The degree of polymerization (DP) is the number of glucose units in the cellulose chain, the DP for the cellulose molecule in Figure 2.2 is $2n+2$. The non-reducing end-group has four hydroxyl groups while an AGU in the cellulose chain has three hydroxyl groups. These hydroxyls are the main reacting groups in cellulose derivatization. The three

cellulose hydroxyls are chemically different, the hydroxyl at position 6 is a primary alcohol and the ones at positions 2 and 3 are secondary alcohols.

### 2.2.1 Hydrogen Bonding and Crystalline Structure

The hydrogen bonding in cellulose (Figure 2.3), has great influence on polymer chain conformation [Kondo, 2004]. In native cellulose the intra-molecular hydrogen bonding occurs both between the O-5 oxygen and the C-3 hydroxyl, and between the O-2 oxygen and the C-6 hydroxyl. The conformation of the $\beta$(1-4) linkage and the specific arrangement of the hydroxyl groups around it facilitates stabilisation by hydrogen bonding. This keeps the AGU from freely rotating and accounts for cellulose being a rigid polymer. Inter-molecular hydrogen bonding, i.e. hydrogen bonding between two molecules occurs between the primary C-6 hydroxyl and the O-3 oxygen on a parallel cellulose chain [Gardner and Blackwell, 1974]. The different hydrogen bonding patterns of cellulose are the basis the different crystalline structures. The rotational conformation of the C-6 hydroxyl group is a significant factor for the hydrogen bonding network. The structure of cellulose I and cellulose II have been intensively studied [O' Sullivan, 1997], since they are the most frequently occurring forms of cellulose. Cellulose I is native cellulose and is characterized by *tg* conformation of O-6 and parallel chain arrangement. Cellulose II has a predominantly *gt* conformation of O-6 and can be obtained by the regeneration of cellulose I. Treatment of cellulose I with the proper concentration of alkali also generates cellulose II, this process is called mercerization. Compounds commonly capable of hydrogen bonding are soluble in water, but cellulose is not water soluble despite that it has three hydroxyl groups on every AGU. It has been argued that inter- and intra-molecular hydrogen bonding does not fully explain the rigidity and insolubility of the cellulose crystal structure [Medronho et al., 2012]. Cellulose molecules have structural anisotropy and are amphiphilic [Yamane et al., 2006], meaning that cellulose has both polar water-soluble parts and hydrophobic water-insoluble parts. This amphiphilicity means that hydrophobic interactions have a role in the cellulose crystal structure. The cellulose I structure in Figure 2.3 only shows intermolecular hydrogen bonding in one plane, creating a sheet-like structure of cellulose molecules. These sheets are

then stacked in a three-dimensional structure [Blackwell, 2012; Gardner and Blackwell, 1974; O' Sullivan, 1997], which is predominantly held together by hydrophobic interactions, a phenomenon called hydrophobic stacking [Bergenstråhle et al., 2010]. The notion that the dissolution characteristics of cellulose are significantly based upon hydrophobic molecular interactions is widely accepted [Warwicker and Wright, 1967; French et al., 1993]. A suitable cellulose solvent would need to be able to break both hydrophobic and hydrophilic bonds, i.e. a solvent must also be amphiphilic in order to solubilize cellulose. As it turns out, many known cellulose solvents are amphiphilic including the ionic liquids used for cellulose dissolution [Hauru et al., 2012].

## 2.3 Cellulose Dissolution and Regeneration

Cellulose regeneration is the process to precipitate cellulose into a desirable form. Cellulose dissolution has been a research field ever since the introduction of modern chemistry in the second half of the $19^{th}$ century, with the aim to create cellulose textile fibers [Woodings, 2001]. In order to convert cellulose to a regenerated fiber, cellulose needs to be dissolved. Cellulose can be dissolved either with a direct solvent or derivatized to an easily soluble cellulose derivative, which after precipitation can be regenerated back to cellulose. The most common derivatizing process is the viscose process, in which cellulose reacts with $CS_2$ to form cellulose xanthate, which is soluble in aqueous alkali. Cellulose is then regenerated in sulfuric acid by hydrolysis of the xanthate groups.A dissolution- and regeneration-process that does not chemically modify cellulose at any stage is called a non-derivatizing process. A direct solvent for cellulose can be either a pure substance or a mixture of different substances, which is more common since cellulose is difficult to dissolve. Solvent mixtures that can dissolve cellulose that are used on a large scale include N-Methylmorpholine N-oxide monohydrate ($NMMO{\cdot}H_2O$) (Lyocell-fiber spinning) and dimethylacetamide / LiCl (DMAc/LiCl) (Gel permeation chromatography solvent). The discovery by Swatloski et al. [2002] that cellulose can be dissolved in some hydrophilic ionic liquids [Swatloski et al., 2002], has sparked research into cellulose regeneration from ionic liquids.

### 2.3.1 Ionic Liquids

Ionic liquids are salts with low melting points. In most ionic liquids bulky organic cations and weakly coordinating anions are used to create molten salts at low temperature. Also, the alkyl chain length of the cation adds a conformational entropic drop in the melting point. Ionic liquids have been called designer solvents because of the many combinations of cations and anions possible [Sheldon, 2005]. According to estimations, it could be possible to synthesize $10^6$ different binary ionic liquids [Rogers and Seddon, 2003]. A positive safety aspect of ionic liquids is that they are usually not flammable, as most volatile organic solvents are. Also, the polarity of ionic liquids is mainly a function of the anion, which can be altered. Another interesting property of ionic liquids is that the vapor pressure is zero or at least negligible. The non-volatility of ionic liquids effectively reduces the risk for environmental release and contamination, in contrast to volatile organic solvents. Ionic liquids have been called green solvents because of these properties [Earle and Seddon, 2000]. However, the non-volatility property is distinct from toxicity and methods for testing environmental and health impact needs to be investigated further before industrial scale use of ionic liquids is possible [Pham et al., 2010]. Also, methods for recycling and reuse of ionic liquid as solvents must be developed.

### 2.3.2 Ionic Liquids for Cellulose Dissolution

The first attempt to use ionic liquids for processing cellulose can be found in a patent from 1934 [Graenacher, 1934]. Graenacher used N-ethylpyridinum as the cation and chloride as the anion to dissolve cellulose. Large scale dissolution of cellulose with N-ethylpyridinium chloride never saw application. Renewed interest in cellulose processing using molten salts occurred in the 2000s when imidazolium based ionic liquids where shown to readily dissolve cellulose at room temperature. Swatloski et al. have shown that 1-butyl-3-methylimidazolium chloride (BMIMCl) can dissolve up to 25% weight cellulose [Swatloski et al., 2002]. The capability to dissolve large amounts of cellulose has also been shown in other imidazolium based ionic liquids [Kosan et al., 2008]. Ionic liquids that are able to dissolve cellulose have high viscosity, and dissolution of cellulose makes the ionic liquid/cellulose solution even more

viscous. One approach to decrease viscosity and improve dissolution dynamics has been to add a co-solvent to the ionic liquid. For instance, adding N-methylimidazole, the precursor for the methylimidazole cation, as co-solvent in methylimidazolium ionic liquids decreases dissolution time and reduces viscosity of cellulose/EMIMAc solutions [Olsson et al., 2014]. The molecular structure for common imadizolium

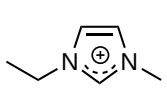

1-ethyl-3-methylimidazolium
Emim

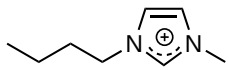

1-butyl-3-methylimidazolium
Bmim

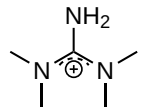


1,1,3,3-tetramethylguanidine
tmg

**Figure 2.4:** *Common ionic liquid cations used for cellulose dissolution. 1-ethyl-3-methylimidazolium acetate is abbreviated EMIMAc*

cations in ionic liquids for cellulose dissolution are shown in Figure 2.4. The alleged non-derivatizing property of EMIMAc as cellulose solvent has been challenged and EMIMAc has been shown to react with cellulose end-groups [Ebner et al., 2008], and also to react with cellulose hydroxyl groups under certain conditions [Köhler et al., 2007].

## 2.4 Rheology

The term rheology means the study of the deformation and flow of matter and it describes the deformation of a body under the influence of stresses. In this context a body is usually a liquid or a gas. The velocity profile of the flow for a given shear stress is controlled by the internal resistance of the liquid, which is called the viscosity of the liquid. For an ideal liquid the viscosity can be described by equation 2.1, which is called Newton's law of viscosity [Bird et al., 2007].

$$\tau = \eta\dot{\gamma} \tag{2.1}$$

The shear viscosity $\eta$, has the unit [Pa s]. The shear rate $\dot{\gamma}$, is the time-derivative of the strain caused by the shear stress acting on the liquid and has the unit [$s^{-1}$] since

the strain $\gamma$ is dimensionless. The viscosities of Newtonian liquids have no shear rate dependence, i.e., the viscosity is constant no matter the shear rate. All other liquids that do not exhibiting this ideal behavior are called non-Newtonian liquids. The viscosity of a non-Newtonian liquids is shear rate dependent and can be described by empirical models like the Carreau model or the Cross model (equation 2.2), which can be used to model polymer solutions [Cross, 1965].

$$\eta = \eta_\infty + \frac{\eta_0 - \eta_\infty}{(1 + (K\dot{\gamma})^m)} \tag{2.2}$$

In the Cross model (equation 2.2), the zero shear viscosity $\eta_0$ [Pa s], is the viscosity at very low shear rate. The asymptotic viscosity at very high shear rate is $\eta_\infty$ [Pa s]. $K$ is a model constant with the unit [s] and $m$ is a dimensionless model constant. The viscosity of polymers in solutions decreases at high shear rates, a behavior that is called pseudo-plastic or more commonly shear thinning. Phenomena like shear thinning is primarily due to changes in the orientation of polymer chains caused by the deformation of the liquid [Barnes et al., 1989a]. For most liquids the shear thinning effect is reversible.

## 2.5 Electrospinning

Electrospinning is based on electrostatic repulsion in a liquid surface. In 1917, John Zeleny published the first photograph of a liquid surface emitting a jet under electrostatic forces [Zeleny, 1917]. The first use of this phenomenon to produce polymer filaments can be found in a 1934 patent by Formhals.Taylor [1964] derived a theoretical model for the phenomenon in 1964, and determined a theoretical conical angle of 49.3° for the drop just before jet formation [Taylor, 1964]. This angle is known as the Taylor angle and the conical shape a liquid surface adapts in an electric field is called a Taylor-cone. Electrospinning produces sub-micron scale fiber filaments. The fundamental mechanism of electrospinning is illustrated in Figure 2.5. In an electrospinning process, a Taylor-cone forms when high voltage is applied to a polymer solution. The liquid surface becomes charged and beyond the Rayleigh charge-limit a fine charged jet of polymer solution emits from the surface. The solvent evapo-

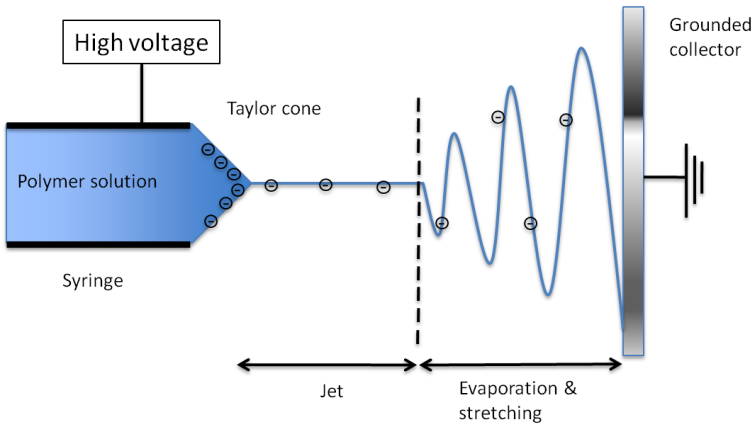


**Figure 2.5:** *Schematic image of electrospinning.*

rates and the jet dries in-flight, forming a fiber. The jet drying time depends highly on initial jet radius [Wu et al., 2011]. The fiber becomes elongated and stretched by whipping and deposits on the grounded collector as a non-woven fiber mat. The stretching of the fiber caused by instability in-flight leads to the formation of thin uniform fibers. Solution properties that influence electrospinning are surface tension, viscosity, conductivity and polymer concentration [Li and Xia, 2004]. Ambient conditions, like temperature and relative humidity, can also influence the electrospinning process [De Vrieze et al., 2009]. Nanofibers are therefore usually electrospun with controlled ambient parameters. Almost any polymer soluble in a volatile solvent can be electrospun. This diversity of electro-spinnable polymers has made this technique attractive for various applications. The term nanofiber is generally used in the scientific literature for electrospun fibers with a diameter smaller than 500 nm [Subbiah et al., 2005]. Fine electrospun nanofibers have a large specific surface area which is very useful in a wide range of applications. Nanofibers are usually collected as non-woven fiber meshes. But several techniques for producing aligned nanofibers have been developed and highly aligned nanofibers have been used in tissue engineering

scaffolds to guide cell growth [Ramakrishna et al., 2006]. The morphology of electrospun nanofibers can be influenced by modifications to the electrospinning process. Porous nanofibers can be created by inducing phase separation inside the nanofiber, for instance by electrospinning mixtures of immiscible polymers and then selectively remove one polymer phase [Greiner and Wendorff, 2007]. Hollow nanofibers or a core-shell nanofiber structures can be formed by co-axial electrospinning. The inherent ability of electrospun nanofibers to mimic the extra cellular matrix (ECM), has made biocompatible nanofibers suitable for use in tissue engineering [Barnes et al., 2007]. Other potential uses are various applications where high porosity is desirable. Electrospun nanofiber can be used as filter media for air filtration. Due to the small fiber diameter even thin transparent air filters can efficiently remove particles [Liu et al., 2015]. Air flow through electrospun nanofibers is also beneficial since the no-slip boundary condition at the fiber surface is not valid for fibers with diameters below 500 nm. This phenomenon is called slip flow and causes low pressure drop over nanofiber filters [Barhate and Ramakrishna, 2007]. Applications for electrospun nanofibers have also been found in electrolyte membranes for energy storage and solar cells [Li and Xia, 2004].

## 2.6 Nanocellulose Derived from Wood

Through mechanical and/or chemical treatment, the native cellulose fiber can be refined to nanocellulose in different forms (Figure 2.6). Cellulose nanocrystals (CNC), also called nanocrystalline cellulose or cellulose whiskers, consist of cellulose crystals extracted from plant tissue. The size of the crystals are 5-70 nm wide and between 100-250 nm long and vary depending the plant source used. CNC are produced through selective acid hydrolysis of the amorphous sections of a cellulose source. Subsequent ultrasonic irradiation creates stable CNC suspensions in water if the CNC are electrostatically stabilized e.g., after sulfuric acid hydrolysis [Ranby, 1951]. The ability of CNC to self-organize into a chiral nematic liquid crystal phase with a helical arrangement above a critical concentration has attracted significant interest [Revol et al., 1992]. Also, the individual rod-like CNC are highly crystalline and have an elastic modulus of 138 GPa [Nishino et al., 1995].

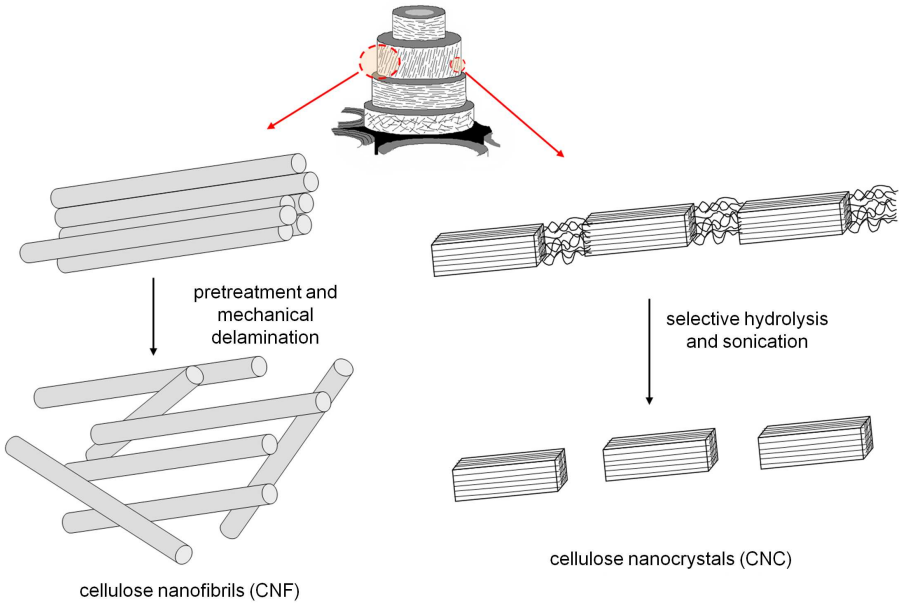


**Figure 2.6:** *Schematic illustration of nanocelluloses derived from wood, cellulose nanofibrils (CNF) and cellulose nanocrystals (CNC), (adapted from [Hasani, 2010], reprinted with permission).*

Cellulose Nanofibrils (CNF), also called nanofibrillated cellulose, or microfibrillated cellulose, can be produced through mechanical treatment of cellulosic pulps in homogenizers [Turbak et al., 1983]. The mechanical treatment causes the pulp fibers to delaminate and liberate the cellulose microfibrils. This mechanical treatment is very energy intensive, which was a major drawback until it was discovered that pretreatments could greatly reduce the high amount of energy needed. Pretreatments have focused on introduction of charged groups in the pulp fiber wall prior to mechanical delamination. These charged groups on the cellulose microfibril surfaces cause electrostatic repulsion between liberated microfibrils. The use of 2,2,6,6-Tetramethylpiperidine 1-oxyl (TEMPO) mediated oxidation as pretreatment improves delamination without changes to the crystallinity. Microfibrils as small widths as 4 nm has been isolated with the use of TEMPO oxidation as pretreatment

[Saito et al., 2006]. Enzymatic pretreatment of cellulose has also been used as pretreatment [Henriksson et al., 2007]. The advantage of CNF compared to pulp fibers is the microfibrils nanometer size which eliminates defects associated with the micrometer structure of pulp fibers. For instance, paper made from CNF has been shown to have very high toughness [Henriksson et al., 2008].

## 2.7 Electrospun Cellulose

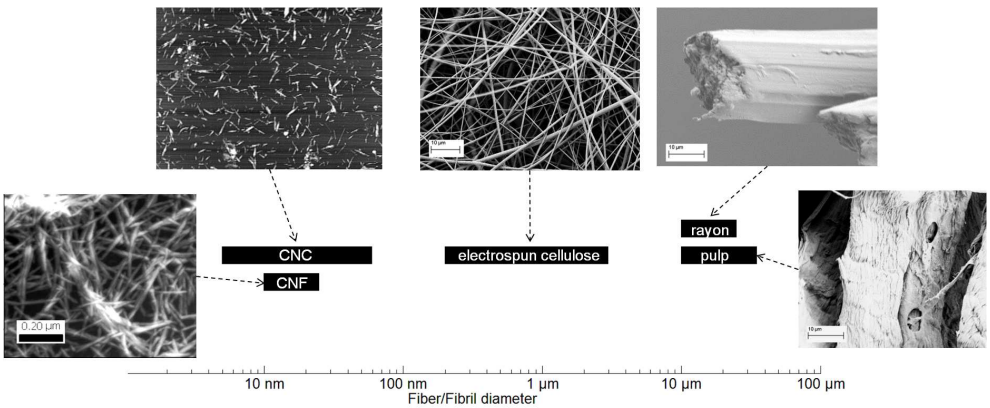


**Figure 2.7:** *Fiber and Fibril diameters of wood based fibrous cellulose.*

Electrospun cellulose nanofibers occupy an intermediate region in terms of fiber/fibril diameter between the nanocelluloses and textile filaments/pulp fibers. This is illustrated in Figure 2.7. Electrospun cellulose nanofibers are continuous and easily handled like man-made celluloses fibers, with the benefits of high specific surface area. Cellulose nanofibers are mostly electrospun using cellulose acetate as polymer and mixtures of acetone as solvent [Liu and Hsieh, 2002; Ma et al., 2005]. The use of cellulose acetate and mixtures of acetone as spinning solution dates back to the first patent by Formhals, who first used electrospinning to produce filaments [Formhals, 1934]. The advantage of this polymer/solvent system is that cellulose acetate is highly soluble in acetone and high polymer concentrations can be used. A

high polymer concentration subsequently generates a high nanofiber output. However, this process generates cellulose acetate nanofibers, which must be regenerated to cellulose. The deacetylation of the nanofibers can be done by alkaline hydrolysis in aqueous NaOH. Cellulose nanofibers generated through this solvent system are usually semi-crystalline with the crystalline parts being Cellulose II polymorph [Kuzmenko et al., 2014]. An electrospinning process which uses cellulose and a direct solvent would therefore be advantageous, since no acetylation and deacetylation steps are needed. Native cellulose has been electrospun from well known cellulose

**Table 2.1:** *Summary of electrospinning conditions used for ionic liquid / cellulose solutions*

| Solvent | Cellulose | Cellulose Conc. | Ref. |
|---|---|---|---|
| BMIMCl/EMIMbensoate | pulp | 10% | Viswanathan et al. [2006] |
| AMIMCl/DMSO | cotton linters | 1-5% | Xu et al. [2008] |
| AMIMCl/DMF | pulp | 1-3.5% | Sui et al. [2008] |
| BMIMCl | micro crystalline | 1.5-5% | Quan et al. [2010] |
| EMIMAc/DMIMCl | cotton linters | 8% | Freire et al. [2011] |
| EMIMAc/DMF | soda pulp of hemp | 14% | Ahn et al. [2012] |

solvents like LiCl/DMAc and NMMO [Kim et al., 2005; Frey, 2008], direct cellulose solvents are not highly volatile, and a coagulation step is required to ensure fiber formation and removal of the solvent from the formed fiber.

Most ionic liquids have a negligible vapor pressure and therefore they do not evaporate. Nevertheless, sub-micron fibers have been electrospun from cellulose dissolved in ionic liquids. Electrospinning relies on solvent evaporation to solidify the fiber, but evaporation cannot occur when the solvent is non-volatile. Different types of celluloses of varying concentrations have been electrospun from non-volatile ionic liquid and these are summarized in Table 2.1. Co-solvents like DMSO and DMF have been used to manipulate spinning solutions properties and decrease viscosity, which seems to improve the electrospinning process. The mechanism of this improved electrospinning is however unclear and no optimal solvent properties have been found. In Paper I, the impact of co-solvents on solution properties of cellulose/EMIMAc solutions was investigated. High boiling point (>150 °C) co-solvents were to manipulate solution properties and the physical properties of the solutions were then correlated to electrospinning performance.

### 2.7.1 Conducting Cellulose Nanofibers

Electrically conductive nanofibers are desirable because they expand the application range for electrospun nanofibers. There have been different approaches to making electrospun nanofibers electrically conductive. For instance, by electrospinning of a conductive polymer using a carrier polymer [Chronakis et al., 2006], or by synthesis of a conductive polymer on already electrospun nanofibers [Lee et al., 2009]. Electrospun cellulose nanofibers have also been carbonized by high temperature heat treatment, which made the resulting nanofibers conductive [Kuzmenko et al., 2014].

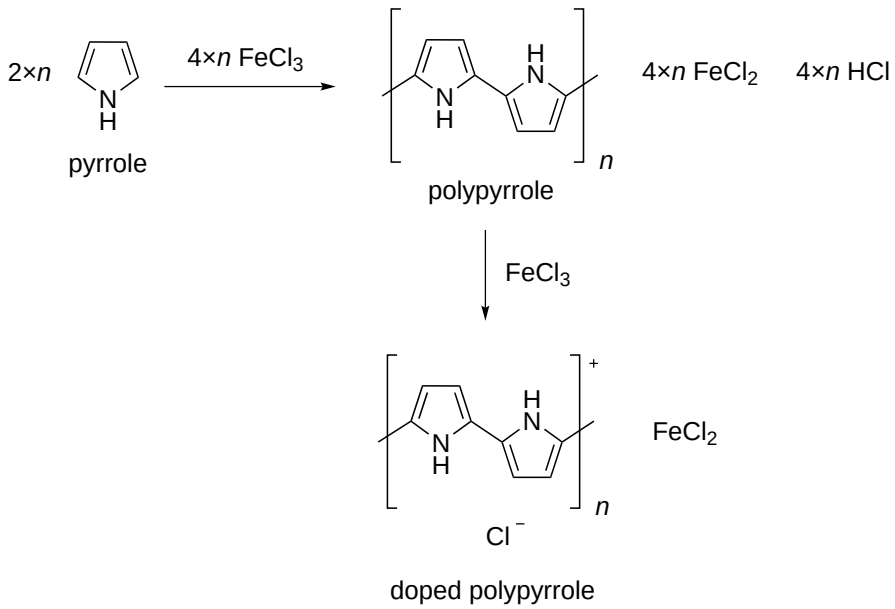


**Figure 2.8:** *Scheme for the synthesis of doped polypyrrole using $FeCl_3$ as oxidant.*

Polypyrrole (PPy) is a conductive polymer that can be easily synthesized from pyrrole monomer (Figure 2.8). PPy can be synthesized by electrochemical methods as films, but for bulk synthesis chemical polymerization using an oxidative reagent is preferable. PPy is a conjugated polymer which consists of a backbone of alternating double and single bonds. This $\pi$-electron configuration makes conjugated polymers

semiconductors and as such they can be doped to increase their conductivity. The backbone chain can lose electrons i.e., be oxidized and its conjugated system gain a delocated positive charge, therefore this type of doping is called p-type doping. Different kind of anionic electrolytes can be used to stabilize the doping. In Figure 2.8 chloride ions are used as anionic counter ion. Effective doping of PPy during polymerization using $Fe_3^+$ based oxidants and electrolytes can increase the conductivity several orders of magnitude. PPy has been investigated for biological applications since it is biocompatible [Bendrea et al., 2011]. The reason for making the surface of tissue engineering scaffolds conductive using PPy is that neural cells can respond to electrical stimulation, which can promote cell differentiation and neurite growth [Schmidt et al., 1997; Guimard et al., 2007; Liu et al., 2009]. For neural tissue engineering purposes, PPy has been previously synthesized on the surface of electrospun nanofibers of poly lactic-co-glycolic acid [Lee et al., 2009]. Moreover, PPy has been synthesized on the surface of porous cellulose for application in energy storage devices [Nyström et al., 2010; Razaq et al., 2012; Carlsson et al., 2012; Wang et al., 2014]. Tissue engineering scaffolds of electrospun cellulose fiber networks can be used to culture cells, both on unmodified cellulose [Jia et al., 2013; He et al., 2014] and on modified cellulose [Rodríguez et al., 2011]. Since PPy adhere to cellulosic materials and electrospun nanofibers are used in tissue engineering, the aim in Paper II was to create electrospun nanofibers and with PPy on its surface to create conductive nanofibers suitable for neural tissue engineering.

## 2.8 Metal-Organic Framework

Metal-organic framework (MOF) materials are coordination networks of metal ions and organic ligands containing potential voids [Batten et al., 2013]. The properties of MOFs depend on the specific metal and ligand used and the three dimensional network structure these form [Öhrström and Larsson, 2005]. MOFs have versatile properties and may potentially have many industrial applications [Mueller et al., 2006; Bétard and Fischer, 2012; Kreno et al., 2012]. The specific micro-porosity of MOF materials have been one focus of interest, since guest molecules can become trapped or adsorbed inside the network voids. Adsorbed molecules can also change

the material properties of the MOF. For instance, certain MOFs can be made electrically conductive by adsorption of certain molecules [Talin et al., 2014]. Also, it has recently been shown that certain MOFs can trap and catalyze the decomposition of nerve agents like Soman [Rosseinsky et al., 2015]. The possibility to tailor-make MOF materials with voids that can adsorb specific molecules opens up possibilities for MOF materials to be used as adsorbent in gas storage and gas separation [Czaja et al., 2009; Férey et al., 2011].

### 2.8.1 Immobilization of MOF

Anionic surfaces have been shown to be beneficial for MOF synthesis. The improved MOF deposition is due to cationic metal anchor points [Zacher et al., 2009; Shekhah et al., 2007; Gliemann and Wöll, 2012]. MOFs have previously been synthesized on natural fiber materials such as silk [Abbasi et al., 2012; Khanjani and Morsali, 2014], cotton [da Silva Pinto et al., 2012; Rodríguez et al., 2014a; Ozer and Hinestroza, 2015] and pulp fibers [Küsgens et al., 2009]. Electrospun fibers have also been used to immobilize MOF, both inside the spun fiber and on the fiber surface [Centrone et al., 2010; Ostermann et al., 2011; Rose et al., 2011; Wu et al., 2012; Jin et al., 2013; Lian et al., 2014]. Lian et al. [2014] synthesized MOF on the surface of electrospun polyurethane nanofibers using toxic and corrosive chromium trioxide to oxidize the nanofiber surface as a pretreatment. A more sustainable approach to a nanofiber/MOF material would be to use nanofibers made from cellulose. However, cellulose has no natural anionic anchor point for the growth of a MOF. In Paper II MOF growth and distribution on the surface of pretreated anionic electrospun cellulose was evaluated.

### 2.8.2 Zeolitic Imidazolate frameworks

One subclass of MOF materials are zeolitic imidazolate frameworks (ZIF), which are based on imidazole ligands and could have future application as membrane material in gas separations [Pimentel et al., 2014]. The name zeolitic imidazolate framework comes from the 145° bridging angle which is present in both ZIFs and zeolites [Park

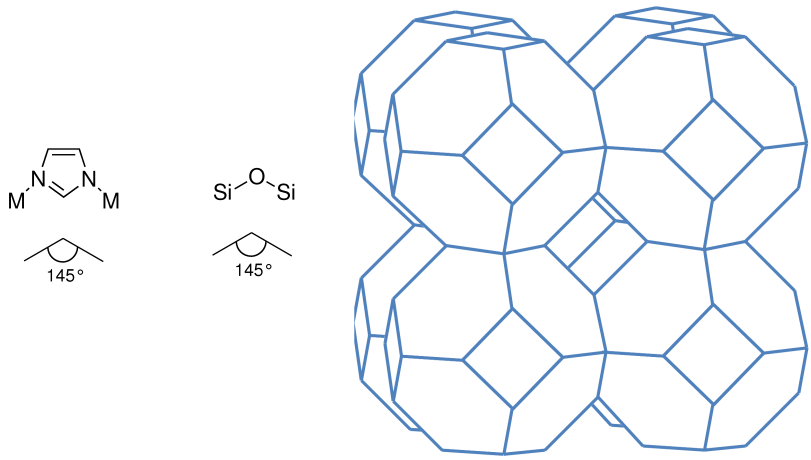


**Figure 2.9:** *The (left) imidazole bridging angle and the (right) extended sodalite net structure.*

et al., 2006]. ZIF-8 has been one of the most studied zeolitic imidazolate frameworks and is built up by Zinc and 2-methylimidazole ligands. The network structure of ZIF-8 is organized together to form cages with 8 hexagonal windows and 6 square windows. These cages are packed together to form the sodalite framework, named after the mineral sodalite where this topology was discovered. The cages formed by the network can act like cavities and host guest molecules. ZIF-8 is a very robust MOF material, with good chemical and thermal stability, that can be synthesized under aqueous conditions[Pan et al., 2011]. Nano-sized ZIF-8 crystals were immobilized using CNF in Paper IV.

# 3

# Materials and Methods

This chapter is a summary of the materials and methods used in the experimental work of this thesis. Further details are available in the appended papers.

## 3.1 Cellulose Sources

High purity dissolving pulp from Domsjö AB, Sweden, was used in electrospinning experiment in Paper I. The number average degree of polymerization (DP) was 750 and determined by size-exclusion chromatography.
Cellulose acetate with an acetyl content of 39.8 wt% and number average molecular weight of 30000 g/mol was used in electrospinning experiment in Paper II and Paper III. Cellulose acatete was deacetylated and back to cellulose after electrospinning.

CNF suspension was prepared according to the method by Okita et al. [2010] 12 g of softwood kraft pulp was suspended in 1200 mL water containing 0.19 g 2,2,6,6-tetramethylpiperidin-1-oxyl (TEMPO) and 1.2 g NaBr. 25.2 mL 2 M NaClO was added to start the oxidation. The reaction was performed at room temperature and pH 10 (the pH was maintained at 10 by addition of 0.5 M NaOH). When no further decrease in pH could be observed the reaction was quenched by addition of 10 mL ethanol. The oxidized pulp was filtered off and thoroughly washed with deionized water. Disintegration to microfibrils was performed with an Ultra-Turrax T 45/N high shear dispersing unit from IKA at 1% pulp consistency at maximal output for 15 minutes, cooling to room temperature every 5 minutes as the suspension temperature rose during the disintegration.

## 3.2 Solvents

Mixtures of the ionic liquid 1-ethyl-3-methylimidazolium acatete (EMIMAc) and co-solvents were used to prepare cellulose solutions in Paper I. Co-solvents used where Dimethyl Sulfoxide (DMSO), Dimethyl Acetamide (DMAc) and Dimethyl Formamide (DMF). Cellulose solutions were prepared by adding co-solvent to dried dissolving pulp followed by addition of EMIMAc, these mixtures were then stirred at 80 °C for 12 h which generated clear solutions.
In Paper II and Paper III a solvent mixture of DMAc:acetone (volume fraction 11:14) was used to create 18 wt% cellulose acetate solutions.

## 3.3 Electrospinning

Electrospinning was performed at constant temperature of 20 °C and constant relative humidity of 65 %. The electrospinning equipment consisted of a high voltage power supply, a NE-1000 syringe pump and a syringe connected to a blunt-nozzle stainless steel needle. A 2.5 cm wide cylindrical (10 cm diameter) grounded collector rotating at 25 rpm was used. The collector was partly submerged in water for electrospinning

experiments involving ionic liquid EMIMAc (Figure 3.1). No waterbath was used in the electrospinning in Paper II and Paper III.

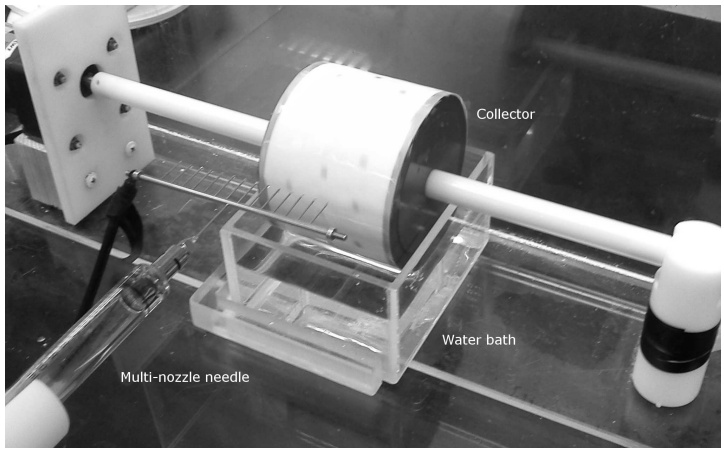


**Figure 3.1:** *Photograph of the electrospinning equipment used.*

## 3.4 Polypyrrole Synthesis

Electrospun cellulose fiber mats were immersed for 3 h in a 0.1 M HCl solution containing 0.05, 0.15 or 0.45 M pyrrole. Then each of the pyrrole soaked cellulose fiber mats were transferred to a 0.1 M HCl solution containing 0.120, 0.360 or 1.08 M $FeCl_3$. Pyrrole was allowed to polymerize for 2 h at 5 °C and then washed thoroughly with deionized water after polymerization to remove excess ions. Washing of the nanofibers mats was stopped when the conductivity of the wash water reached below 0.25 mS/cm. The color of the nanofiber mats changed from white to black during PPy synthesis.

## 3.5 Cell Study

Prior to the cell study in Paper II, a cytotoxicity analysis was performed in accordance with ISO standard 10993-5:2009(E) Annex C to investigate potential cytotoxicity of the cellulose/PPy nanofiber materials. The details of this analysis can be found in the supporting information of Paper II. Cell studies on nanofiber materials were performed using human neuroblastoma cells (SH-SY5Y) obtained from Health Protections Agency Culture Collections and are described in detail in Paper II.

## 3.6 Anionic Cellulose Nanofibers

Electrospun cellulose nanofibers were made anionic in Paper III to facilitate MOF synthesis. Two methods for introducing carboxyl groups on the cellulose nanofiber surface were used. Cellulose nanofiber mats were treated with 5% w/v NaOH solution and sodium chloroacetate (1 M). The mats were washed several times with deionized water and then finally with ethanol. The second method used carboxymethyl cellulose, CMC, which was adsorbed on cellulose nanofiber mats using a method previously published by Rodríguez et al. [2011]. Briefly, cellulose nanofiber mats were immersed in an aqueous solution containing sodium carboxymethyl cellulose (250 mg/L) and $CaCl_2$ (0.01 M) for 24 h. The samples were then immersed in $CaCl_2$ solution (0.1 M) for 24 h to introduce calcium counter ions to the surface. The samples were then washed thoroughly with deionized water. The role of $CaCl_2$ was to enhance the irreversible adsorption of CMC on to the cellulose surface [Laine et al., 2000].

## 3.7 MOF Synthesis

In Paper III, the MOF HKUST-1 [Chui et al., 1999], $[Cu_3(C_9H_3O_6)_2]$, was synthesized on nanofibers using a layer-by-layer approach. Nanofiber mats were immersed in copper acetate solution (1 mM) of ethanol:DMF (1:1 v/v) for 15 min

and then washed with ethanol:DMF. After washing, the mats were immersed in 1,3,5-benzenetricarboxylic acid (1 mM) for 30 min and then washed again with ethanol:DMF solvent. These four steps formed one cycle. The ethanol:DMF solution was changed into fresh solution after every fifth cycle and metal salt/ligand solutions were freshly prepared after every eight cycles. The nanofiber mats were washed with ethanol:DMF solution after synthesis and dried in ambient conditions.
In Paper II, the MOF ZIF-8, $[Zn(C_4H_6N_2)_2]$, was synthesized on CNF. CNF suspension was added to 20 mL of 5 M 2-methylimidazole under stirring. The volume of this CNF/ligand solution was then adjusted to 35 mL with deionized water. 0.238 g (0.8 mmol) $Zn(NO_3)_2$ was dissolved in 5 mL deionized water and added to the CNF/ligand solution under stirring, a white solid precipitated and a clear upper phase separated. The precipitate was centrifuged, (4000 rpm, 15 min) separated and re-suspended in deionized water several times to remove excess 2-methylimidazole. The suspended precipitate was then frozen with liquid nitrogen dried in a freeze under high vacuum, yielding free standing CNF/MOF hybrid materials.

## 3.8 Characterization

This section describes the analysis instruments used in this thesis.

### 3.8.1 Solution Properties

Viscosity measurements using shear stress sweeps were performed on a Bohlin Rheometer CS 30. The measurements were conducted using a cone-and-plate geometry with a diameter of 25 mm and a cone angle of 5.4° at room temperature. Steady state shear viscosity was measured at shear stresses in the range 0.24-370 Pa.
Surface tension was measured using the pendant drop technique. The instrument used was a VCA Video Contact Angle System 2500. The software VCAOptimaXC was used to capture the image of the pendant drop and to fit the curvature of the drop to the Young-Laplace equation. Conductivity was measured with a CON 5/TDS 5 Conductivity meter (Eutech Instruments).

### 3.8.2 Nanofiber Properties

Water contact angles were measured using sessile droplet technique on an Attension Theta contact angle meter (Biolin Scientific). The electrical conductivity measurements were performed using a two-point probe system (Parameter Analyzer-Keithley 4200-SCS).
X-ray photoelectron spectroscopy (XPS) was performed using a Quantum 2000 scanning XPS microprobe. An Al K$\alpha$ (1486.6 eV) X-ray source was used and the analyzed area was approximately $500 \times 500$ $\mu m^2$ with a depth of 4-5 nm.
Fourier transform infrared spectroscopy (FTIR) spectra were collected with a Perkin Elmer 2000 FT-IR using an attenuated total reflection module (ATR), which enabled sample surfaces to be examined without further preparation.
Thermogravimetric Analysis (TGA) was performed with a Perkin Elmer TGA 7 using $N_2$ as purge gas. Samples were dried at 160 °C before analysis and the temperature gradient was 5 C°/min.
Two different instruments were used to collect X-ray diffraction (XRD) patterns, a Siemens Diffractometer D5000 and a Bruker D8 Advance diffractometer. Multipoint Brunauer-Emmett-Teller (BET) surface areas were measured by two different instruments. A Quantachrome instruments Autosorb-1c and a Micromeritics Tristar 3000.

### 3.8.3 Microscopy

Two different scanning electron microscopes (SEMs) were used to study nanofiber morphology. A JEOL JSM-5300 and a LEO Ultra 55 FEG SEM. All samples were gold sputtered in a vacuum for 80 s at 10 mA before SEM analysis. The atomic force microscopy (AFM) used in Paper II was a Digital Instrument Nanoscope IIIa with a type G scanner. The cantilever used was a Micro Masch silicon cantilever NSC 15. The measurements were performed in air using tapping mode.

# 4

# Cellulose Electrospun from Ionic Liquids

This chapter describes the findings in Paper I. In this paper co-solvents were used to modify the viscosity, electrical conductivity, and surface tension of cellulose/EMIMAc solutions. The solution properties were then correlated to electrospinning performance.

## 4.1 Electrospinning of Cellulose/Ionic Liquid Solutions

The polymer concentration influence the zero shear viscosity of cellulose solutions. In dilute solutions, concentration dependence is linear, but in concentrated solutions

$\eta_0$ can be described by a power law function. The concentration at which the viscosity dependence changes is called the critical overlap concentration, $c^*$ and depend on the average cellulose DP [Blachot et al., 1998]. In Figure 4.1, this dependence is shown for two celluloses with different DP. Cellulose solutions with low viscosities

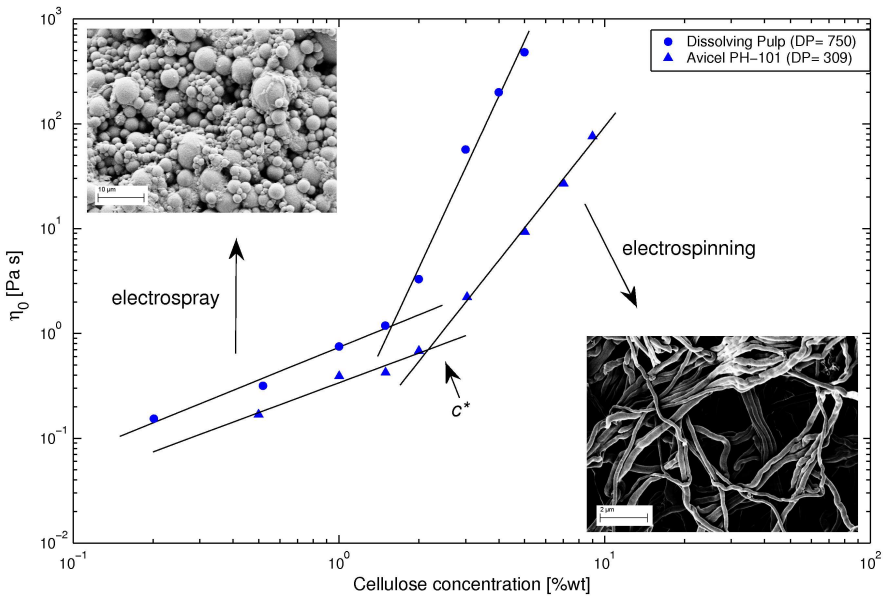


**Figure 4.1:** *Zero shear viscosity cellulose/EMIMAc solutions plotted as a function of concentration, c* is the critical overlap concentration. Inset are SEM images of cellulose nanofibers made by electrospinning and spherical cellulose particles made by electrospray.*

below $c^*$ can electrospray, which generates spherical particles instead of nanofibers. In Paper I, cellulose solutions of 2.5 % dissolving pulp were made using ionic liquid EmimAc and co-solvents DMSO, DMAc and DMF according to Table 4.1. This cellulose concentration is above $c^*$ in Figure 4.1. The cellulose solutions were electrospun for 1 h using a electrospinning setup which included precipitation bath. In Figure 4.2, a high speed photograph of an experimental electrospinning test is shown. The formation of the fibers seems to be chaotic, i.e. the fibers can be seen forming close to the needle and then accelerating towards the collector. The morphology of

**Table 4.1:** *Solutions prepared for electrospinning*

| | | Solvent mixture | |
|---|---|---|---|
| Sample solution[a] | Co-solvent | Co-solvent [%wt] | EMIMAc [%wt] |
| Pulp:IL:DMF-9[b] | DMF | 90 | 10 |
| Pulp:IL:DMF-7 | DMF | 70 | 30 |
| Pulp:IL:DMF-5 | DMF | 50 | 50 |
| Pulp:IL:DMF-3 | DMF | 30 | 70 |
| Pulp:IL:DMF-1 | DMF | 10 | 90 |
| | | | |
| Pulp:IL:DMAc-9[b] | DMAc | 90 | 10 |
| Pulp:IL:DMAc-7 | DMAc | 70 | 30 |
| Pulp:IL:DMAc-5 | DMAc | 50 | 50 |
| Pulp:IL:DMAc-3 | DMAc | 30 | 70 |
| Pulp:IL:DMAc-1 | DMAc | 10 | 90 |
| | | | |
| Pulp:IL:DMSO-9 | DMSO | 90 | 10 |
| Pulp:IL:DMSO-7 | DMSO | 70 | 30 |
| Pulp:IL:DMSO-5 | DMSO | 50 | 50 |
| Pulp:IL:DMSO-3 | DMSO | 30 | 70 |
| Pulp:IL:DMSO-1 | DMSO | 10 | 90 |
| | | | |
| Pulp:IL | -[*] | 0 | 100 |

[a] Cellulose pulp concentration by weight in solution mixtures was 2.5%. [b] Cellulose insoluble in mixture, samples were not electrospun. [*] Reference sample containing only EMIMAc and cellulose pulp.

electrospun samples was characterized using SEM and classified according to the fibers formed. In order to assess the electrospinning performance of the different solutions, fiber formation was ranked. Examples of the different fiber morphologies are shown in Figure 4.3. These fiber images represent the three most common depositions collected after electrospinning. In Table 4.2 samples from all co-solvent solutions are categorized according to the classifications in Figure 4.3. The trend in Table 4.2 clearly shows that the best fiber forming was with the DMSO-based solvent mixtures. For these solvent mixtures the best fiber formation was between 50

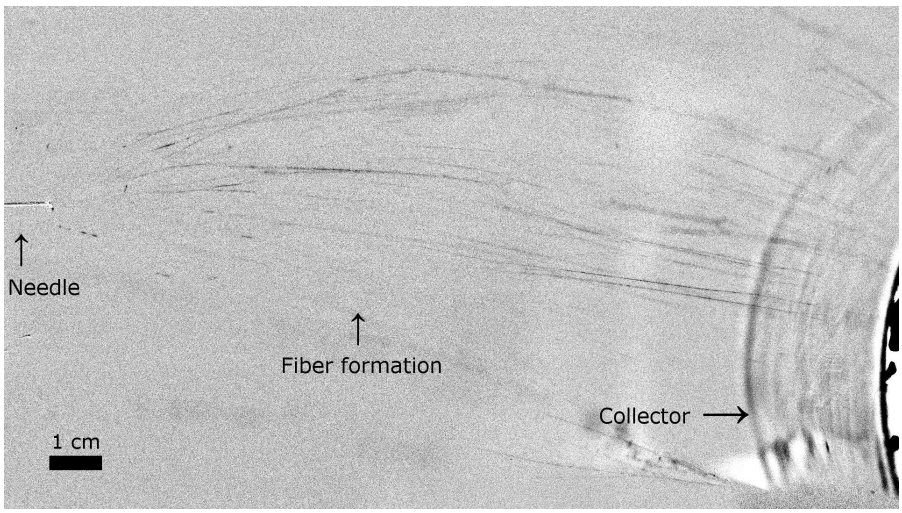


**Figure 4.2:** *Photograph of electrospinning of cellulose/EMIMAc/DMF solution. Photograph recorded with a Prosilica GE 6180 high-speed camera using stroboscope at 125 Hz. The needle and the collector are visible.*

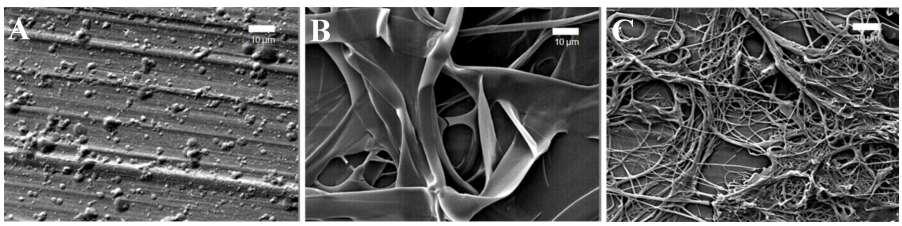


**Figure 4.3:** *SEM images of electrospun cellulose (A) no nanofiber formation; (B) tendencies to form nanofibers and (C) nanofiber formation (©2012 Wiley Periodicals Inc, reused with permission).*

and 70 wt % EMIMAc. It can also be seen that all three solvent mixtures needed a high content of EMIMAc to form fibers, but not too high, since pure EMIMAc did not give the best fiber formation. For the DMAc- and DMF-based solvent mixtures the best fiber formation was at 90 wt % EMIMAc.

**Table 4.2:** *Evaluation of electrospun solutions*

| | Nanofiber formation[a] | | |
|---|---|---|---|
| Sample solution | Run # 1 | Run # 2 | Run # 3 |
| Pulp:IL:DMF-9 | - | - | - |
| Pulp:IL:DMF-7 | + | + | + |
| Pulp:IL:DMF-5 | + | + | + |
| Pulp:IL:DMF-3 | + | ++ | +++ |
| Pulp:IL:DMF-1 | +++ | +++ | +++ |
| | | | |
| Pulp:IL:DMAc-9 | - | - | - |
| Pulp:IL:DMAc-7 | + | + | + |
| Pulp:IL:DMAc-5 | + | + | + |
| Pulp:IL:DMAc-3 | + | + | + |
| Pulp:IL:DMAc-1 | ++ | ++ | +++ |
| | | | |
| Pulp:IL:DMSO-9 | + | + | +++ |
| Pulp:IL:DMSO-7 | +++ | + | +++ |
| Pulp:IL:DMSO-5 | +++ | +++ | +++ |
| Pulp:IL:DMSO-3 | +++ | +++ | +++ |
| Pulp:IL:DMSO-1 | +++ | ++ | +++ |
| | | | |
| Pulp:IL | +++ | ++ | ++ |

[a] (-) Sample could not be electrospun, (+) no fiber formation, (++) Fiber formation tendencies,(+++) Fiber formation. For example images see Figure 4.3.

## 4.2 Properties of Cellulose/Ionic Liquid Solutions

Surface tension, conductivity and viscosity was measured on the electrospinning solution and characterization details are available in the experimental section of Paper I. A low surface tension is favorable for electrospinning [Greiner and Wendorff, 2007]. Surface tension is plotted against the molar fraction EMIMAc in the Figure 4.4 for all electrospinning solutions. The surface tension decreases with addition of co-solvent. DMF and DMAc are more effective than DMSO in reducing surface tension. Also, the surface tension seems to be linearly dependent on co-solvent fraction The DMSO-

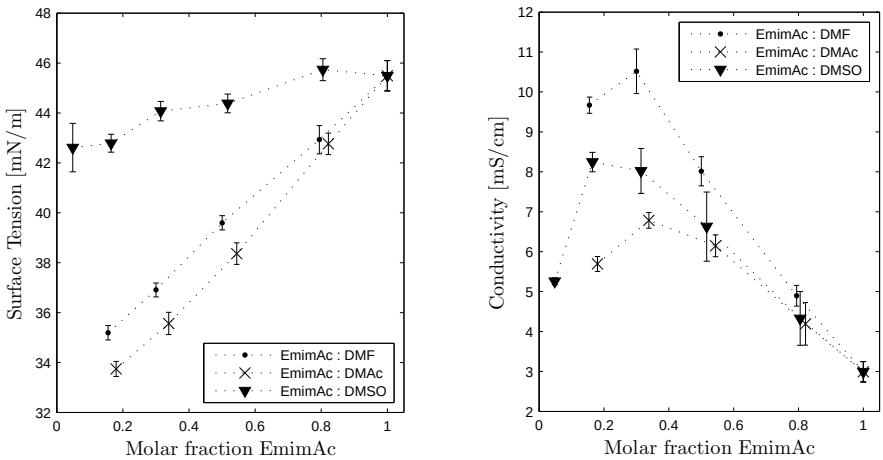


**Figure 4.4:** *Mean values of (left) surface tension and (right) conductivity of electrospun solutions.*

based solvent mixtures had the highest surface tension regardless of molar fraction EMIMAc and were also the most favorable co-solvent (Table 4.2). Fibers could be electrospun from solutions with a surface tension greater than 42 mN/m, regardless of co-solvent. Since a low surface tension is favorable for electrospinning and the easily electrospun solutions had the highest surface tension, it can be concluded that surface tension is not a limiting factor for the solution mixtures tested in this study.
A high conductivity is favorable for electrospinning, since the mobility of ions is crucial for the accumulation of ions at the liquid surface and the subsequent forming of a Taylor-cone. Conductivity is plotted against the molar fraction EMIMAc for the different co-solvents mixtures in Figure 4.4. All three solvent systems appear to have a maximum conductivity depending on the molar fraction EMIMAc. For solutions containing DMF the peak is around 0.3 molar fraction EMIMAc, for DMAc as the co-solvent the peak is around 0.35, and for DMSO as the co-solvent the peak is around 0.18. Solutions containing DMF have the highest conductivity and solutions containing DMAc the lowest. In Figure 4.4 and Table 4.2 it can be seen that solutions that formed fibers are in the conductivity range of 3 to 8 mS $cm^{-1}$. However,

there were also unsuccessful solutions in that conductivity range and since the DMF and DMAc mixtures that could be electrospun have conductivity, it can be concluded that conductivity is not a limiting factor for the solution mixtures tested here. Also, all of the solutions tested are in the mS/cm range, which mean that they were highly conductive solutions.

In Figure 4.5, viscosity as a function of shear rate is shown for the electrospun

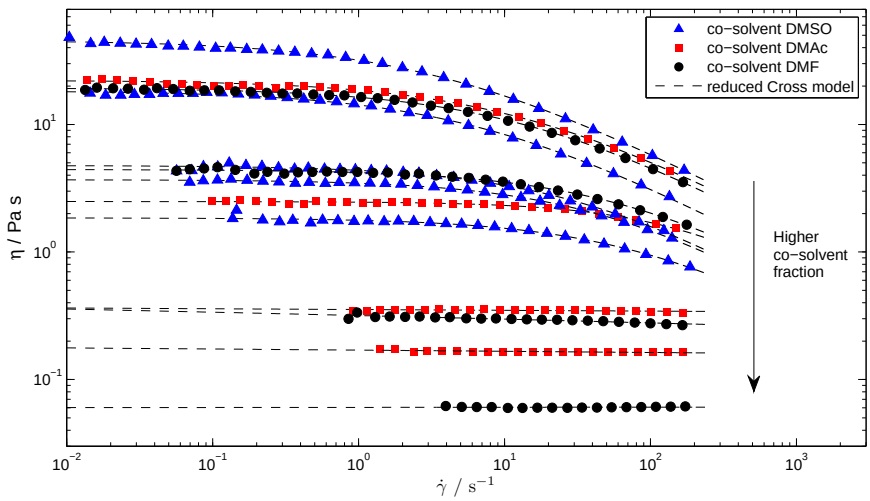


**Figure 4.5:** *Viscosity as a function of shear rate on cellulose dissolved in EmimAc with DMSO, DMAc and DMF as co-solvent at different ratios. Viscosity data shown with markers and reduced Cross model with dashed lines.*

EmimAc/co-solvent solutions in run #3 (Table 4.3). At high fractions of EmimAc, the solutions are shear thinning and the viscosity decreases with increasing amount of co-solvent. DMSO does not decrease viscosity as efficient as DMAc and DMF, which at the low fractions of EmimAc seem to even reduce the shear thinning property of the solutions. This is an indication that polymer conformation and entanglement is unchanged by shear stress and therefore not present in the solutions with DMF and DMAc in a co-solvent fraction above 50 %wt.

$$\eta = \frac{\eta_0}{(1 + (K\dot{\gamma})^m)} \tag{4.1}$$

The rheometer used could not measure viscosity at shear rates above 200 $s^{-1}$ and the asymptotic viscosity at high shear rates $\eta_\infty$ was not determined. The viscosities could however be modeled by a reduced Cross model (equation 4.1) [Barnes et al., 1989b]. This model was fitted to the viscosity data using the least squares method and is also plotted in Figure 4.5. The model (equation 4.1) uses three parameters to

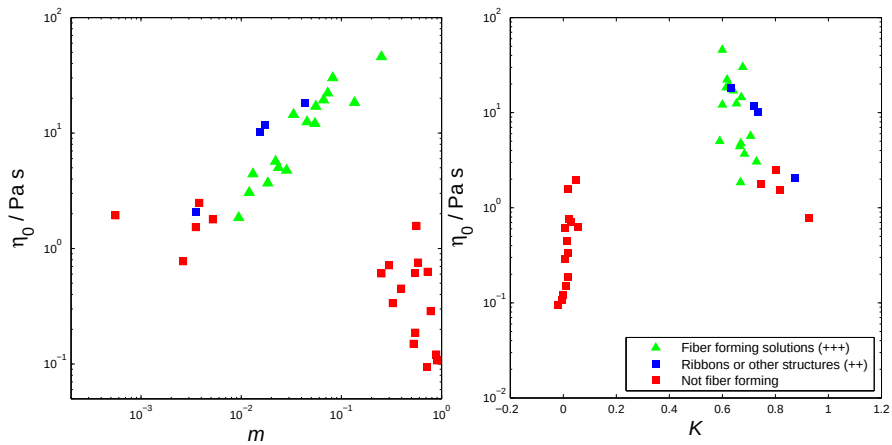


**Figure 4.6:** *Zero shear viscosity, $\eta_0$ plotted against Cross model constants (left) $m$ and (right) $K$. Electrospun solutions that yielded fibers are marked as green triangles.*

estimate the viscosity as a function of shear rate, the zero shear viscosity $\eta_0$ and the constants $K$ and $m$. All successfully electrospun solutions had a zero shear viscosity in the 2-44 Pa s range. However, there were also unsuccessful solutions in that viscosity range. By plotting the zero shear viscosity against the two model constants (Figure 4.6), regions with all the successfully electrospun solutions appear, regardless of what co-solvent was used. Fiber forming solutions had exponential constant $0.01 < m < 0.2$, $0.6 < K < 0.8$ and $2 < \eta_0 < 44$, which indicate that both a high viscosity and high shear thinning is beneficial for electrospinning from non-evaporating solvents like EmimAc. These results indicate that a high viscosity at low

shear rates could be beneficial for the formation of a stable Taylor-cone, while a low viscosity at the high deformation rates present in the emitted jet could be preferable for the elongation of emitted jets. For most of the non fiber forming solutions the $K$ constant was approaching 0, the $m$ constant was close 1 and the $\eta_0$ was below 2 Pa s, which mean that solutions both had low shear thinning and low viscosity.

## 4.3 Conclusions of Paper I

Solution properties were studied and correlated to fiber formation when electrospinning cellulose from ionic liquid EMIMAc. Co-solvents DMSO, DMAc and DMF were used to manipulate solution properties. Co-solvents could decrease viscosity and surface tension of cellulose solutions. The rheological properties of electrospun cellulose solutions could be linked to fiber formation. A high zero shear viscosity together with a high shear thinning was beneficial for fiber formation.

# 5

# Chemical Modification of Cellulose Nanofibers

This chapter describes the methods and discusses the findings in Paper II and Paper III. In these papers cellulose nanofibers were electrospun and chemically functionalized to give the resulting nanofiber materials new properties.

## 5.1 Polypyrrole Synthesis on Cellulose Nanofibers

Cellulose nanofibers were electrospun using the cellulose acetate/DMAc/acetone solvent system and experimental details are available in Paper II. PPy was synthesized on cellulose nanofibers using $FeCl_3$ as both oxidative polymerization reagent and

as doping reagent in a one pot reaction (Figure 2.8). Different concentrations were used to create different loadings of PPy on the nanofibers. The concentration ratio pyrrole:$FeCl_3$ in the monomer and reagent solutions were 1:2.4. The nanofiber mats changed color from white to black during PPy synthesis.

### 5.1.1 Properties and Microstructure of Cellulose/PPy nanofibers

**Table 5.1:** *Summary of results of the characterization of electrospun scaffold materials*

| | | Element composition (XPS) | | | | Conductivity | Contact |
|---|---|---|---|---|---|---|---|
| Material Sample | Py conc.[a](M) | C% | N% | O% | Cl% | (S/cm) | Angle[b] |
| Cellulose | - | 54.53 | - | 45.47 | - | $7.8*10^{-7}$ | 14.6° |
| Cellulose/PPy 0.05 | 0.05 | 62.67 | 7.31 | 29.00 | 1.01 | $5.7*10^{-2}$ | 10.6° |
| Cellulose/PPy 0.15 | 0.15 | 62.69 | 7.82 | 28.95 | 0.54 | $2.6*10^{-4}$ | 15.5° |
| Cellulose/PPy 0.45 | 0.45 | 66.31 | 14.45 | 18.70 | 0.55 | $5.2*10^{-4}$ | 22.6° |

[a] Pyrrole concentration used in the *in situ* polymerization. [b] Advancing water contact angle.

Different PPy loadings were achieved by the use of different concentrations of pyrrole monomer in the PPy synthesis. The element compositions in Table 5.1 were extracted from X-ray photoelectron spectroscopy (XPS). Full XPS spectra and resolved C1s peaks of cellulose nanofibers and cellulose/PPy nanofibers are shown in Figure 5.1, four peaks are resolved C-C (284.4 eV), C-O and C-N (285.8 eV), O-C-O (287.2 eV) and O-C=O (288.6 eV) [Beamson and Briggs, 1992]. The small O-C=O peak indicate that small amounts of acatate is still present in the cellulose nanofibers after deacetylation. The effect of pyrrole polymerization can be seen in the appearance of nitrogen and chlorine peaks. Also, the increased intensity of the C-C peaks in the resolved XPS spectra indicate deposition of PPy on the nanofibers. PPy is a nitrogen and carbon containing polymer and as anticipated, both the nitrogen and carbon content increased as the concentration of reactants was increased. A rise in conductivity can be seen in cellulose/PPy nanofiber materials compared to the unmodified cellulose nanofibers (Table 5.1). The increase in conductivity for the cellulose/PPy nanofiber materials confirmed the presence of conductive PPy at the nanofiber surface.

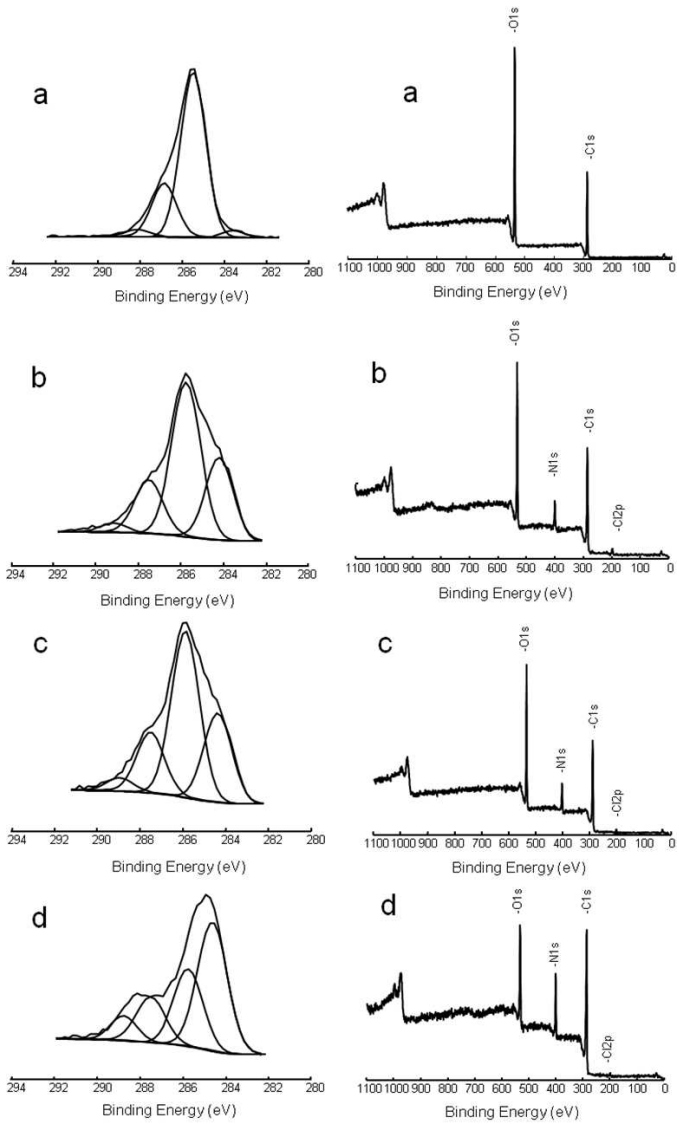


**Figure 5.1:** *Resolved C1s peaks and full XPS spectra of (a) cellulose nanofiber, (b) cellulose/PPy 0.05, (c) cellulose/PPy 0.15 and (d) cellulose/PPy 0.45.*

The material synthesized with the lowest concentration of pyrrole, 0.05 M, displayed the highest increase in conductivity compared to unmodified cellulose nanofibers. This may seem counterintuitive, but this material also had the highest chlorine dopant content with 1%, which indicate that this material had the highest content of oxidized conductive PPy. Also, a $FeCl_3$ concentration above 0.1 M has been shown to cause over-oxidation of PPy, which reduce conductivity [Kaynak and Beltran, 2003]. The cellulose/PPy materials polymerized with high pyrrole and $FeCl_3$ concentrations may suffer the drop in conductivity due to over-oxidation. The increased intensity of the O=C-O peaks in Figure 5.1 (c and d) suggests that these samples were over-oxidized. SEM images of the electrospun cellulose nanofibers revealed that their

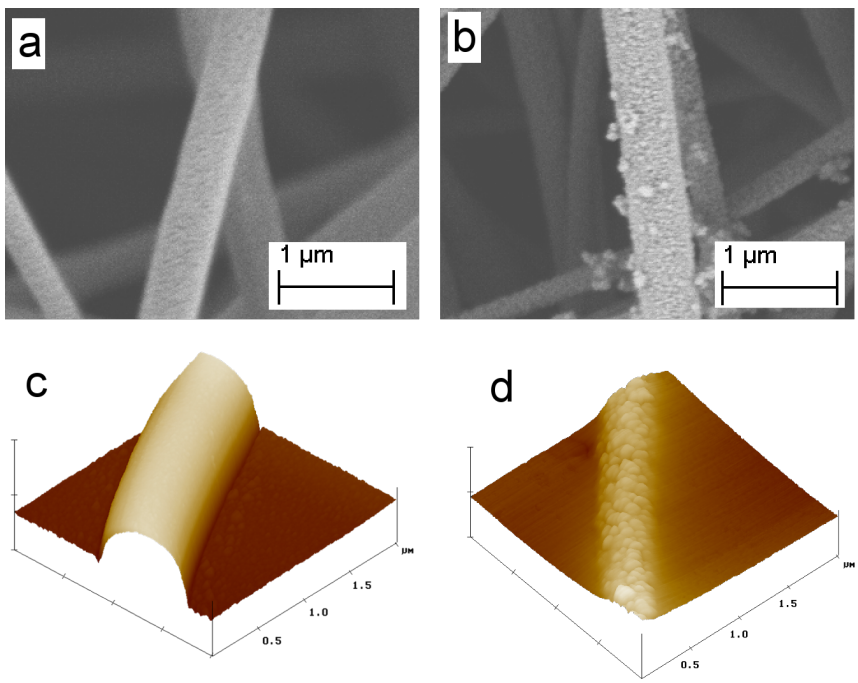


**Figure 5.2:** *SEM images of (a) a single electrospun cellulose nanofiber and (b) a single nanofiber of cellulose/PPy 0.05. AFM images of (c) a single electrospun cellulose nanofiber and (d) a single nanofiber of cellulose/PPy 0.05. AFM scan area was 2×2 µm.*

diameter ranged between 300 nm and 1500 nm. Furthermore, SEM and high resolution AFM images of single nanofibers of cellulose and cellulose/PPy show small PPy particles adhering to the nanofiber surface (Figure 5.2). The unmodified cellulose nanofiber has a very smooth surface, while nano sized PPy particles seem to cover the whole cellulose/PPy nanofiber surface, consequently making the surface rougher. In addition, PPy particles seem to be evenly distributed on the surface, providing continuous conductive material. The effect of pyrrole concentration in the

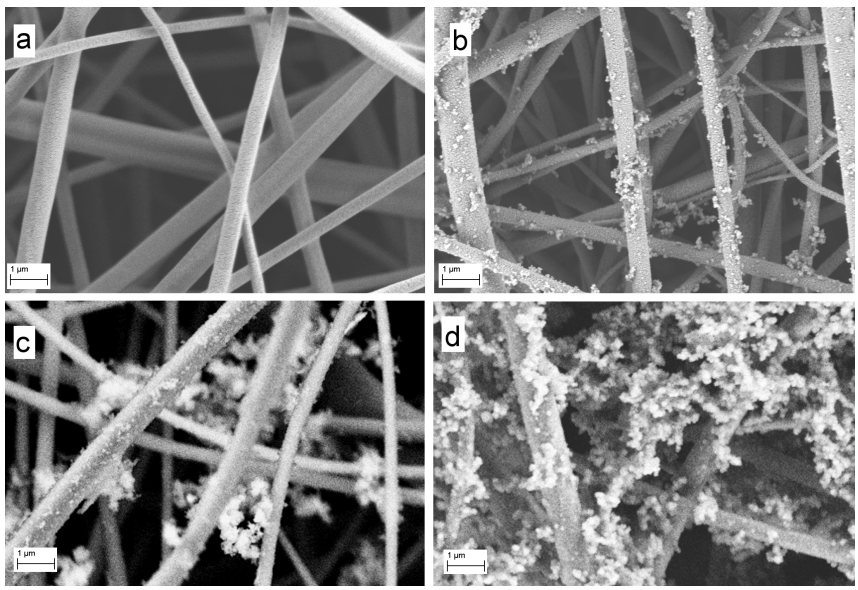


**Figure 5.3:** *SEM images of (a) electrospun cellulose nanofiber, (b) cellulose/PPy 0.05, (c) cellulose/PPy 0.15 and (d) cellulose/PPy 0.45. Scale bars are 1* µm *(©2015 Springer Science+Business Media Dordrecht, reused with permission).*

PPy synthesis can be seen in Figure 5.3. If a low concentration of pyrrole was used (0.05 M), the nanofiber materials have mostly small PPy particles adhering to the nanofiber surface. But as pyrrole concentration increases PPy particles seem to form freely in voids of the nanofiber network. These PPy particles seem to cluster together and reduce the macro-porosity of the overall nanofiber material.

### 5.1.2 Cell Growth on Cellulose/PPy nanofibers

A cytotoxity test using fibroblast cells revealed that none of the cellulose/PPy nanofibers had cytotoxic potential. Details of this assessment are available in Paper II. The cellulose/PPy 0.05 nanofiber material was used for neural cell culture since it had the highest conductivity, a nanofibers structure without clusters of PPy particles (Figure 5.3). SH-SY5Y human neuroblastoma cells were seeded on the scaffolds and after 48 hours of culture, differentiation was initiated by medium change. SEM images of SH-SY5Y cell morphology at three time points are shown in Figure 5.4. After

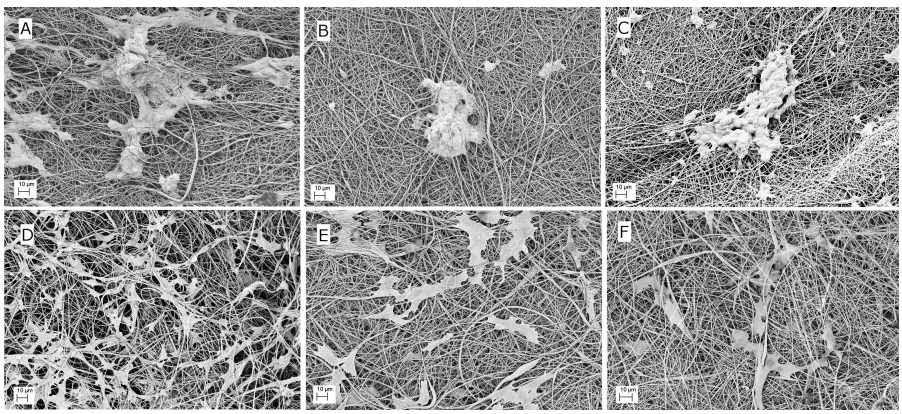


**Figure 5.4:** *SEM images of SH-SY5Y cells differentiated on cellulose nanofibers (a) day 5, (b) day 10, (c) day 15; Cellulose/PPy nanofibers (d) day 5, (e) day 10, (f) day 15. Scale bars are 10*$\mu m$

5 days of differentiation, cells on the unmodified cellulose nanofiber scaffold had a tendency to form aggregates and to attach to each other. The same phenomenon was observed on day 10 and day 15. On the cellulose/PPy scaffolds, SH-SY5Y cells have a more even distribution on the nanofibers scaffold, which could indicate improved cell adhesion. On day 10 and 15 the cells continue to exhibit integration on the cellulose/PPy scaffolds. The morphological characteristics of SH-SY5Y also differ on the two different materials. Cells on the unmodified cellulose nanofiber scaffold had a spherical shape, while the morphological characteristics point towards a more

neuron-like phenotype on the cellulose/PPy scaffolds. The mechanism behind the differences in cell adhesion and cell morphology in the PPy coated scaffolds is however unclear. Pyrrole was evenly polymerized on the cellulose nanofibers resulting into a continuous conductive material. The nano-scale surface roughness induced by the PPy coating could favor cell attachment to the nanofibers since surface roughness favors cell adhesion [Fonner et al., 2008]. It has also been shown that tumor cells have adhesion preference to nano rough surfaces compared to smooth surfaces [Chen et al., 2013]. The synthesis of PPy introduced amine groups to the nanofibers surface, which could have influenced the neural cell performance. Amine containing polysaccharides like chitosan have been show to be suitable for neural tissue engineering [Prabhakaran et al., 2008; Cooper et al., 2011]. The passive conductive property of substrates for neural tissue engineering have been studied by Malarkey et al., who compared neural cell growth on films with similar roughness but with different conductivity. Films substrates of certain conductivity (0.3 S/cm) slightly promoted neurite outgrowth [Malarkey et al., 2009]. The conductivity of the scaffold material used (0.057 S/cm) is unlikely to have an effect on neural cell performance.

### 5.1.3 Conclusions of Paper II

PPy was successfully in situ synthesized on the surface of electrospun cellulose nanofibers which rendered a conductive material mimicking an ECM. The conductivity and the microstructure were affected by the synthesis parameters used. SEM and AFM showed that PPy adhered to the nanofiber surface as small particles, which increased the surface roughness of the nanofibers. Increased pyrrole concentration in the PPy synthesis did not increase the thickness of the PPy coating, but caused PPy to freely form as clusters. The non-toxic property of electrospun cellulose was retained after PPy synthesis. Neural cell culture experiment indicated that PPy enhanced SH-SY5Y cell adhesion and on electrospun cellulose/PPy nanofiber scaffolds. SH-SY5Y cell viability was evident up to 15 days of differentiation in the cellulose/PPy scaffolds, which opens up possibilities for this cellulose based material to be utilized as neural tissue engineering scaffolds.

## 5.2 MOF Functionalized Cellulose Nanofibers

This section describes the methods and discusses the findings in Paper III. In this work cellulose nanofibers were made anionic in order to improve synthesis of Metal-organic frameworks on the nanofibers.

### 5.2.1 Synthesis of MOF Functionalized Nanofibers

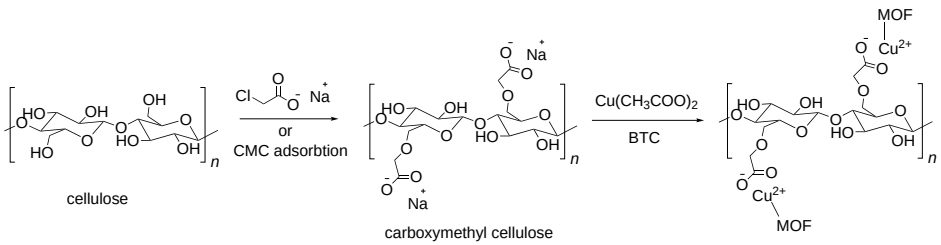


**Figure 5.5:** *Scheme for synthesis of HKUST-1 on carboxymethylated and CMC adsorbed cellulose nanofibers*

Cellulose nanofibers were electrospun using the cellulose acetate/DMAc/acetone solvent system and experimental details are available in Paper III. Carboxylate groups were thereafter introduced to the cellulose nanofiber surface by two different methods, reaction with sodium chloroacetate and adsorption of carboxymethyl cellulose. The MOF HKUST-1 [Chui et al., 1999], also known as $Cu_3(BTC)_2$, was subsequently synthesized on the pretreated cellulose nanofibers using a layer-by-layer approach. In this approach copper ions and 1,3,5-benzenetricarboxylic acid ligands were introduced in cycles to form HKUST-1, which could coordinate to the cellulose surface (Figure 5.5). The number of synthesis cycles used were 8 and 32, in order to investigate the dynamics of HKUST-1 deposition on the nanofibers. The presence of HKUST-1 was verified with XRD and ATR FTIR. The XRD patterns of all the HKUST-1 functionalized cellulose nanofibers are shown in Figure 5.6, together with the XRD pattern of pure HKUST-1 and a HKUST-1 reference pattern (CSD-DIHVIB [Yakovenko et al., 2013]) generated by the software Mercury 3.3. The high similar-

ity of these patterns proves the formation of HKUST-1 in all the cellulosic nanofiber materials. The general trend in Figure 5.6 indicates an increased intensity of the characteristic HKUST-1 peaks as the number of synthesis cycles increase. XRD peaks at 12°, 20° and 22° are associated with Cellulose II polymorph structure [Fink et al., 1995]. The broad peaks at $2\theta$=20° in the cellulose nanofiber samples confirms the semicrystalline state of electrospun cellulose generated via the DMAc/acetone solvent system with subsequent deacetylation [Rodríguez et al., 2014b; Kuzmenko et al., 2014]. ATR FTIR spectra of all the HKUST-1 functionalized cellulose nanofibers

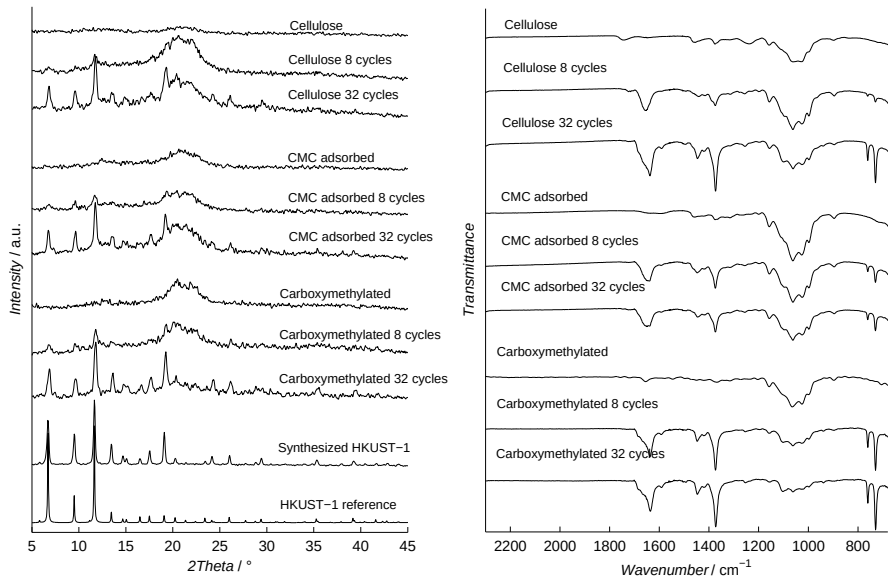


**Figure 5.6:** *(left) XRD patterns of HKUST-1/nanofiber samples and reference patterns, (right) ATR FTIR spectras of HKUST-1/nanofiber samples.*

show strong characteristic vibration bands at 729 $cm^{-1}$, 760 $cm^{-1}$, 1373 $cm^{-1}$, 1447 $cm^{-1}$ and 1637 $cm^{-1}$ (Figure 5.6). These vibration bands were in good agreement with published data on HKUST-1 [Li and Yang, 2008]. The broad vibration band at 1200-900 $cm^{-1}$ that stems from the cellulose seem to decrease in intensity as the number of synthesis cycles increase, which indicate that both HKUST-1 and

cellulose is present in the nanofiber material.

**Table 5.2:** *Cellulosic nanofiber samples treated with layer-by-layer HKUST-1 synthesis method*

| | HKUST-1 content[a] | |
|---|---|---|
| Material type | 8 cycles | 32 cycles |
| Carboxymethylated | 11.8% | 38.7% |
| CMC adsorbed | 9.2% | 38.9% |
| Plain cellulose | 9.8% | 32.2% |

[a] HKUST-1 content was estimated from thermogravimetric analysis data and described in detail in paper III.

The HKUST-1 contents in Table 5.2 show a linear dependence on the number of synthesis cycles. The loading of HKUST-1 can be easily controlled by the number of synthesis cycles. The anionic pretreatment seems to have a limited effect on HKUST-1 loading, which is dependent of the number of synthesis cycles.

### 5.2.2 Properties of MOF Functionalized Nanofibers

SEM images reveal HKUST-1 on the surface of all HKUST-1 functionalized cellulose nanofibers and as anticipated there were differences in the HKUST-1 deposition between the different nanofibers. HKUST-1 crystals are visible on the surface of non-pretreated plain cellulose nanofibers after 8 cycles (Figure 5.7 a ), and after 32 cycles the nanofibers appear to be unevenly covered by HKUST-1 (Figure 5.7 b ). Partly covered nanofibers are also visible in the CMC adsorbed nanofibers (Figure 5.7 d ), which indicate adhesion of HKUST-1 to CMC treated nanofibers was low. It is also possible that the HKUST-1 had uneven crystal growth on these surfaces due to fewer carboxylate anchor points. The carboxymethylated nanofibers, on the other hand, display a uniform growth of HKUST-1 over the whole nanofiber surface, both in the 8 cycle sample and the 32 cycle sample (5.7 e and f ). This observation in the carboxymethylated nanofibers indicate that carboxylate anchor points are evenly distributed on the nanofibers surface and that adhesion between the

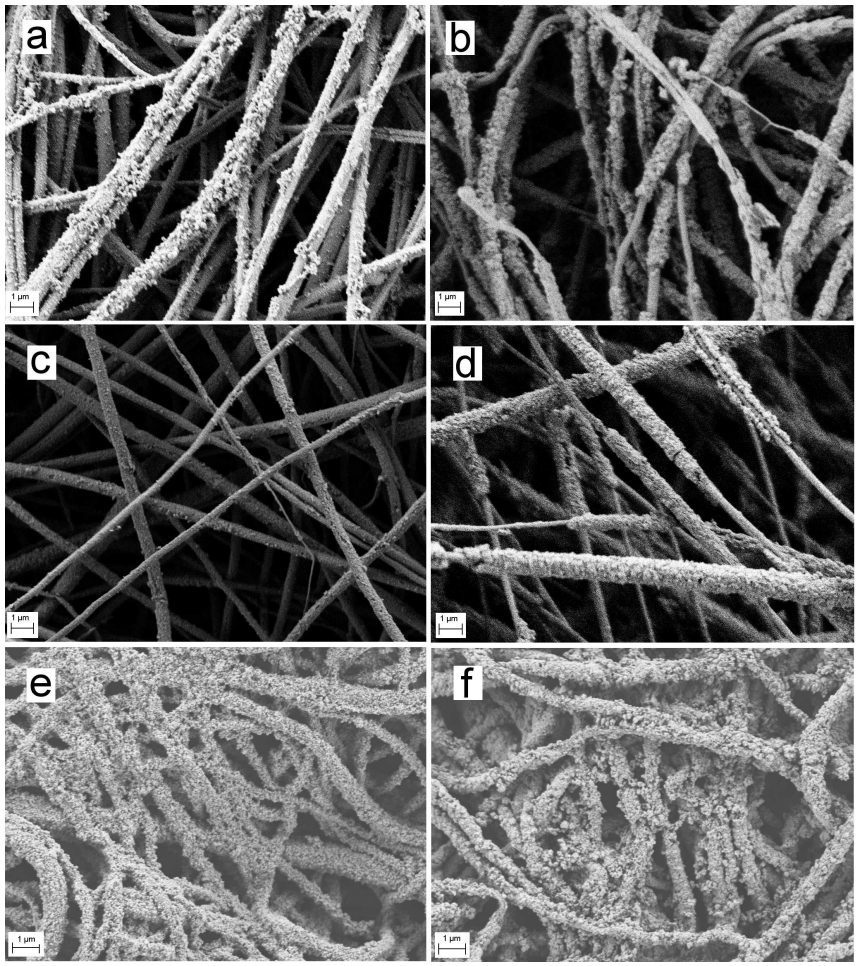


**Figure 5.7:** *SEM images of (a) cellulose nanofibers 8 synthesis cycles, (b) cellulose nanofibers 32 synthesis cycles, (c) CMC adsorbed nanofibers 8 synthesis cycles, (d) CMC adsorbed nanofibers 32 cycles, (e) carboxymethylated nanofibers 8 cycles, (f) carboxymethylated nanofibers 32 cycles, scale bars are 1 µm. (©2015 WILEY-VCH Verlag GmbH & Co reused with permission).*

nanofibers and HKUST-1 is high. The carboxymethylated nanofibers appear more densely packed and curved, which can be attributed to the swelling of cellulose by a high concentration of NaOH during the carboxymethylation. $N_2$ adsorption measurements were made in order to confirm high porosity properties of the HKUST-1 functionalized cellulose nanofibers. The specific surface area was determined using the Brunauer-Emmett-Teller (BET) multipoint method and details are available in Paper III. Carboxymethylated cellulose nanofibers functionalized with 32 HKUST-1 synthesis cycles was used since this nanofiber material had high HKUST-1 content that was evenly distributed on the nanofiber surface. The BET surface area was 440 $m^2\ g^{-1}$ for the HKUST-1 functionalized cellulose nanofibers, while only 10 $m^2\ g^{-1}$ for the unmodified cellulose nanofibers. HKUST-1 materials have been synthesized on other cellulose materials. Küsgens et al. reached a HKUST-1 loading of 19.9% and a BET surface area of 314 $m^2\ g^{-1}$ on paper pulp fibers in a one-pot synthesis [Küsgens et al., 2009]. The higher loading of HKUST-1 presented in this work indicates that a larger surface is accessible for MOF functionalization in electrospun nanofibers than in pulp fibers.

### 5.2.3 Conclusions of Paper III

HKUST-1 was synthesized on pretreated anionic electrospun cellulose which gave the resulting MOF/cellulose material a nano-porous structure suitable for gas adsorption. The anionic pretreatment did not enhance the loading but had impact on distribution HKUST-1. The carboxymethylated electrospun cellulose was best suited for HKUST-1 functionalization, since the HKUST-1 crystals became evenly distributed on the nanofiber surface. The approach of surface modification of cellulose for the synthesis of MOF/cellulose materials presented in this work opens up possibilities for MOF synthesis on other cellulose materials, such as CNF.

# 6

# MOF Functionalized CNF

This chapter describes the methods and discusses the findings in Paper IV. In this work the concept of synthesizing MOFs on cellulose was transferred to another type of nano structured cellulose, TEMPO oxidized CNF.

## 6.1 ZIF-8 synthesis on CNF

The zeolitic imidazole framework ZIF-8 has been synthesized under aqueous conditions, which makes it applicable for functionalization of cellulose nanofibrils. Pan et al. found that a high concentration ratio of [2-methylimidazole] / [$Zn^{2+}$] was necessary for the formation of ZIF-8 in water [Pan et al., 2011; Tanaka et al., 2012; Kida et al., 2013]. The use of water as reaction medium for MOFs open up the possibil-

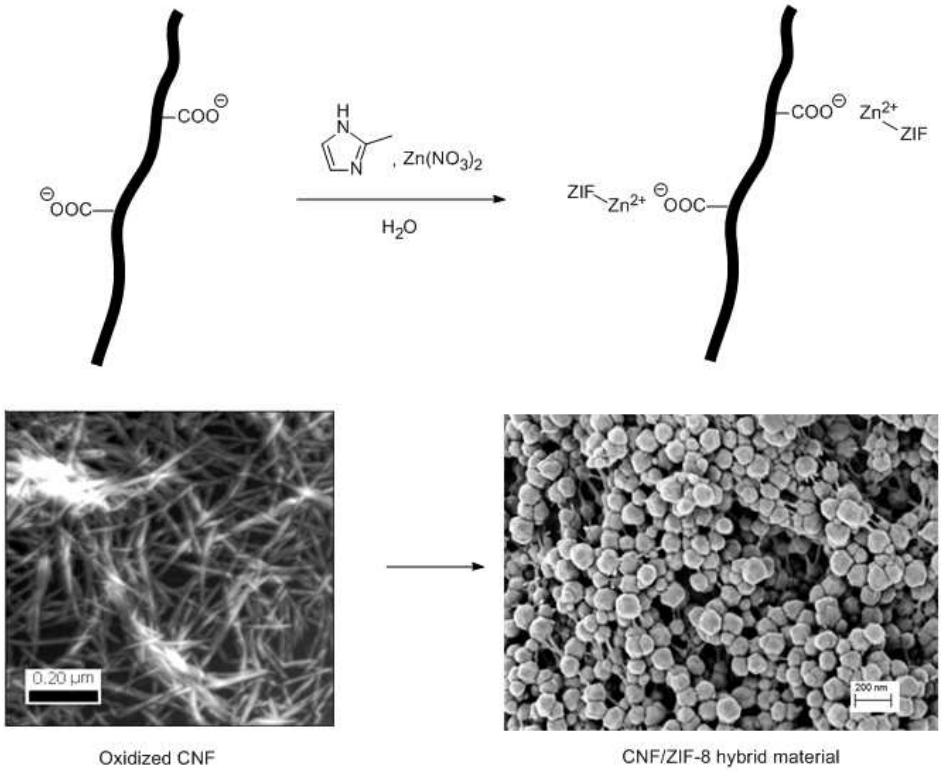


**Figure 6.1:** *Scheme for synthesis of ZIF-8 on oxidized CNF.*

ity to easily synthesize MOFs on cellulose and especially on CNF, since CNF are extracted from cellulose pulp as water based suspension. In addition, a water based synthesis has the potential to be inexpensive and easy to scale up.

TEMPO oxidized CNF were prepared according to the method by Okita et al. and described in detail in paper IV. ZIF-8 was synthesized by addition of $Zn(NO_3)_2$ to aqueous solutions CNF/2-methylimidazole, which caused CNF and ZIF-8 to precipitate (Figure 6.1). Free standing ZIF-8/CNF hybrid materials were created by freeze drying. The ZIF-8/CNF hybrid materials were more brittle than plain freeze dried CNF. Different loadings of CNF were used in the synthesis in order to re-

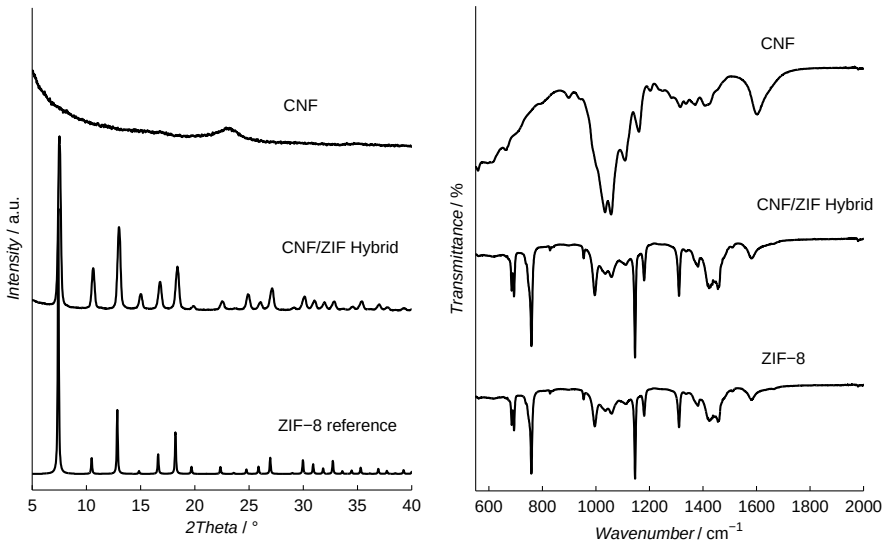


**Figure 6.2:** *XRD patterns and FTIR spectra of CNF, CNF/ZIF-8 hybrid material and pure ZIF-8.*

ceive CNF/ZIF-8 materials with different loading of ZIF-8. The presence of ZIF-8 was confirmed with XRD and FTIR. The XRD patterns of CNF and the CNF/ZIF-8 hybrid materials are shown in 6.2, together with a ZIF-8 reference pattern (CSD-FAWCEN [Morris et al., 2012]) generated by the software Mercury 3.3. The XRD pattern proves the formation of ZIF-8 of sodalite topology in the CNF/ZIF-8 hybrid materials. In 6.2 characteristic ZIF-8 vibration bands at 695 $cm^{-1}$, 758 $cm^{-1}$, 995 $cm^{-1}$, 1148 $cm^{-1}$, 1180 $cm^{-1}$ and 1310 $cm^{-1}$ are visible for the ZIF-8/CNF hybrid materials, these are consistent with published FTIR data of ZIF-8 [Park et al., 2006; Pan et al., 2011]. The cellulose polysaccharide vibration bands at 1034 $cm^{-1}$, 1056 $cm^{-1}$, 1110 $cm^{-1}$ and 1160 $cm^{-1}$ are clearly distinguishable for the CNF. Also, a vibration band at 1600 $cm^{-1}$ in the CNF sample can be attributed to C=O stretching [Schwanninger et al., 2004] and confirms the oxidized state of CNF. In both the FTIR and XRD data the ZIF-8 is dominating in the hybrid materials, which was anticipated

**Table 6.1:** *BET surface area of CNF functionalized with ZIF-8.*

| Sample | CNF[a] | ZIF-8 content[b] [% wt] | BET surface area [$m^2$ $g^{-1}$] |
|---|---|---|---|
| CNF/ZIF Hybrid | 3g | 79.7 | 1014.1 |
| CNF/ZIF Hybrid | 5g | 68.8 | 527.9 |
| CNF | - | - | 31.5 |

[a] Amount of CNF used in each sample.

[b] Estimated from Zn content.

since the loading of ZIF-8 was high. The BET surface area of plain freeze dried CNF was 31.5 $m^2$ $g^{-1}$, while the surface area of the CNF/ZIF-8 hybrid material with the highest loading of ZIF-8 was 1014.1 $m^2$ $g^{-1}$ (Table 6.1). Tanaka et al. reported a BET surface area of pure aqueous synthesized ZIF-8 of 1600 $m^2$ $g^{-1}$, this means that a higher BET area for a material with 79.7% ZIF-8 loading is possible, which indicates that there might be some impurities in the ZIF-8 or that solvent from the synthesis still occupy voids in ZIF-8. Lian et al. reached a loading of 63% and a BET surface area of 566 $m^2$ $g^{-1}$ on electrospun polyurethane nanofibers. The results presented here shows that a higher ZIF-8 content is possible when going from electrospun nanofibers to smaller fibrils with CNF.

A picture of a free standing freeze dried CNF/ZIF-8 hybrid material is shown in Figure 6.3. The CNF/ZIF-8 hybrid material was light and porous, like a CNF aerogel. Also shown in Figure 6.3 is a SEM image of the CNF/ZIF-8 hybrid material surface. The surface seems to be covered by nano-sized ZIF-8 crystallites and the cellulose fibrils are clearly visible in between. A fractured surface of CNF/ZIF-8 hybrid material show what seems to be cellulose fibril structures together with nano-sized ZIF-8. The fibrils seem to be evenly distributed throughout the material and can act as reinforcement and hold the nano-sized ZIF-8 particles together. Both the CNF and the ZIF-8 crystallites have nano scale dimensions and the fibril diameter is smaller than the diameter of the ZIF-8 crystallites. MOFs have been synthesized on other cellulose materials like pulp fibers [Küsgens et al., 2009] and cotton [da Silva Pinto et al., 2012; Lange and Obendorf, 2015; Ozer and Hinestroza, 2015]. The use of nano-sized fibrils to immobilize MOFs creates a more uniform homogeneous material without the hierarchical structure of micrometer sized fibers.

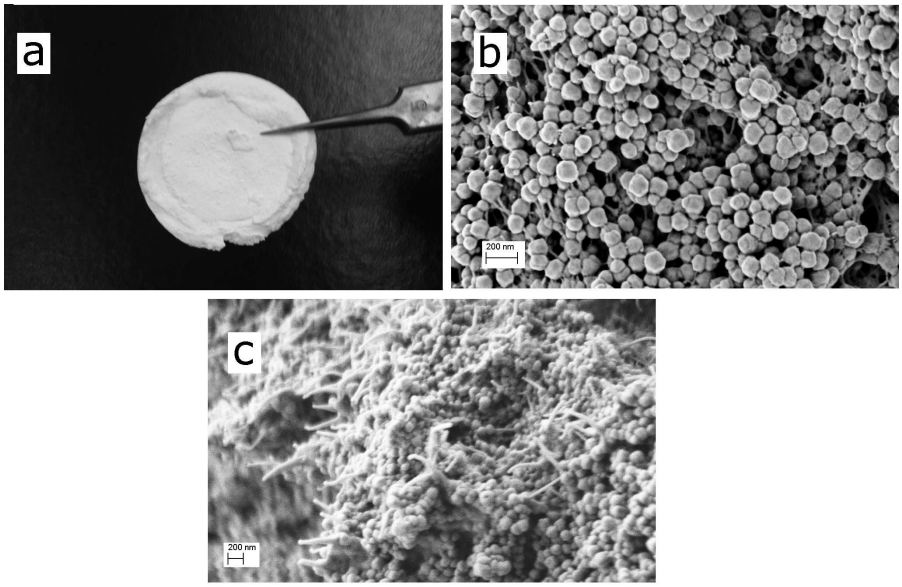


**Figure 6.3:** *Digital photograph of (a) CNF/ZIF-8 Hybrid, SEM image of (b) CNF/ZIF-8 Hybrid, SEM image (c) of fractured surface of CNF/ZIF-8 Hybrid, scale bars in the SEM images are 200 nm.*

## 6.2 Conclusions of Paper IV

ZIF-8 was synthesized on TEMPO oxidized CNF in aqueous medium and highly porous ZIF-8/CNF hybrid materials could be created by freeze drying. However, optimal strength and loading of ZIF-8 for a potential gas storage or gas separation/storage membrane require further studies. Also, optimal structure and charge density of the CNF needs to be evaluated. The approach of using a nanocellulose to immobilize ZIF-8 is straightforward and has the potential to be easily scaled up. In addition, other MOFs can by this method be used to give nanocellulose materials new properties.

# 7

# Concluding Remarks and Future Outlook

## 7.1 Electrospun Cellulose from Ionic Liquids

The fiber formation in electrospinning is based on solvent evaporation. Ionic liquids can be used for electrospinning cellulose, despite having negligible vapor pressure. In this thesis it has been shown that fiber formation is connected to viscosity, for non-evaporating solvents in electrospinning. One inherent problem in the scale-up of electrospinning is low output of nanofibers. Therefore a high polymer concentration is preferable. This is a drawback for cellulose solutions since cellulose is difficult to dissolve in high concentrations and the resulting solution is usually very

viscous. Ionic liquids can probably be utilized in other types of spinning processes where evaporation of volatiles might be an issue, like wet-spinning or air-gap spinning. In electrospinning however, the non-evaporating property is a drawback that limits the use ionic liquids. Ionic liquids can perhaps be useful in mathematical modeling of electrospinning jets since the evaporation phenomenon can be neglected.
The search is still on for a solvent that allows for one-step electrospinning of cellulose nanofibers via direct dissolution, without coagulation or derivatization steps. The route of electrospinning cellulose through a derivative like cellulose acetate in solvent mixtures of acetone is still the main solvent system for producing electrospun cellulose nanofibers. The deacetylation step is a drawback for this system but the advantages is the high polymer concentration and the ease of electrospinning from a volatile solvent. The path forward for electrospun cellulose can be to utilize the nanocelluloses to improve the electrospinning process and nanofiber strength. CNCs can form stable suspensions which can be electrospun with addition of a carrier polymer, which can improve the cellulose content of the spinning solution. Also, CNCs are highly crystalline and have high elastic modulus which could improve nanofiber strength.

## 7.2 Conducting Cellulose Nanofibers

PPy was successfully synthesized on the surface of electrospun cellulose nanofibers which rendered the nanofibers conductive. PPy adhered to the nanofiber surface as small particles, which increased the surface roughness of the nanofibers. The conductivity and the microstructure were affected by the synthesis parameters used. PPy particles formed freely and clustered together when high concentration pyrrole mononer was used. Futher optimization of the polypyrrole synthesis could improve conductivity of the nanofiber material. Also, other dopants could be used to improve conductivity.
Electrospun nanofiber can mimics an ECM and have therefore potential use in the field of tissue engineering. The non-toxic property of electrospun cellulose was retained after PPy synthesis. Neural cell culture experiments indicated that PPy enhanced SH-SY5Y cell adhesion and on cellulose/PPy nanofiber scaffolds and cell

viability was evident up to 15 days of differentiation. Future work would include more cell studies on these conductive nanofibers in combination with electric stimulation to improve cell performance and neurite growth. Future work could also focus on electrospinning of aligned nanofibers, which could guide cell growth, perhaps in combination with electric stimulation to build neural networks.
The PPy functionalized cellulose nanofibers are not limited to use only as tissue engineering scaffolds. Other potential applications could be pressure sensitive sensors, functional textiles and high surface area electrodes.

## 7.3 MOF functionalized cellulose materials

MOFs have emerged as a family of highly porous materials that possess a broad array of potential applications. Potential uses include gas purification, storage, separation and catalysis. The immobilization of MOF materials is vital for its use in potential future applications. It was shown in this work that cellulose nanofibers could be excellent carriers of MOF particles when made anionic. Also, it was shown that the nanocellulose CNF could be used to immobilize MOFs in an one-step synthesis in aqueous medium. This open up possibilities to create cellulose based materials with specific absorbent properties. Also, this synthesis is inexpensive and environmentally sound, since only a salt, ligand and water is used. The imidazole ligand must however be able to be recycled and reused since it is used in excess. Future work would include evaluation of the strength and elastic modulus of the CNF/ZIF-8 materials. Also, finding optimal ZIF-8 loading and optimal CNF characteristics could improve material characteristics. Finding a suitable application could also be a path forward. For instance one where the MOF material can acts a catalyst or adsorbent of a specific gas.

# 8

# Acknowledgments

The research in this thesis has been made possible by the Knut and Alice Wallenberg Foundation trough the Wallenberg Wood Science Center.

First and foremost I want to thank my advisor Prof. Gunnar Westman for being an excellent guide to the world of science.

I am also very grateful to Prof. Gunnar Westman and Prof. Paul Gatenholm for giving me the opportunity to be a Ph.D. student.

I also want to thank all the co-authors of the papers for their expertise and effort.

I want to thank Agnes Stepan, Johan Sundberg, Tuve Mattson, Karl Håkansson and Jonas Wetterling for excellent help in the lab.

I want to thank Prof. Per Lincoln and the rest of the management at KB Chalmers for help and support.

Past and present members of the Westman research group at Chalmers are also acknowledged for all their help and fruitful discussions. I especially want to thank Dr. Merima Hasani for proofreading this thesis. Also, all the great Ph.D. students and scientists in the WWSC are acknowledged for making the WWSC courses & conferences so great.

I also want to thank my family, especially Elin, for her support and encouragement.

# List of Abbreviations

AGU Anhydrous Glucose Unit, page 6

AMIMCl 1-Allyl-3-methylimidazolium chloride, page 16

BMIMCl 1-Butyl-3-methylimidazolium chloride, page 9

BTC 1,3,5-benzenetricarboxylic acid, page 44

CNC Cellulose Nanocrystals, page 13

CNF Cellulose nanofibrils, page 14

DMAc Dimethyl Acetamide, page 22

DMF Dimethyl Formamide, page 22

DMIMCl 1-Decyl-3-methylimidazole chloride, page 16

DMSO Dimethyl Sulfoxide, page 22

DP Degree of Polymerization, page 6

ECM Extra Cellular Matrix, page 13

EMIMAc 1-Ethyl-3-methylimidazolium acetate, page 22

HKUST-1 Hong Kong University of Science and Technology-1, page 24

MOF Metal-Organic Framework, page 18

NMMO N-Methylmorpholine N-oxide, page 8

PPy Polypyrrole, page 17

SEM scanning electron microscopy, page 26

TEMPO 2,2,6,6-Tetramethylpiperidine 1-oxyl, page 14

WWSC Wallenberg Wood Science Center, page 2

ZIF Zeolitic Imidazolate Frameworks, page 19

# Bibliography

Abbasi, A., Akhbari, K., and Morsali, A. (2012). Dense coating of surface mounted CuBTC metal-organic framework nanostructures on silk fibers, prepared by layer-by-layer method under ultrasound irradiation with antibacterial activity. *Ultrasonics Sonochemistry*, 19(4):846–852.

Ahn, Y., Lee, S., Kim, H., Yang, Y.-H., Hong, J., Kim, Y.-H., and Kim, H. (2012). Electrospinning of lignocellulosic biomass using ionic liquid. *Carbohydrate Polymers*, 88(1):395–398.

Barhate, R. and Ramakrishna, S. (2007). Nanofibrous filtering media: Filtration problems and solutions from tiny materials. *Journal of Membrane Science*, 296:1 – 8.

Barnes, C. P., Sell, S. A., Boland, E. D., Simpson, D. G., and Bowlin, G. L. (2007). Nanofiber technology: Designing the next generation of tissue engineering scaffolds. *Advanced Drug Delivery Reviews*, 59(14):1413 – 1433.

Barnes, H. A., Hutton, J. F., and Walters, K. (1989a). *An introduction to rheology*, chapter 6. Elsevier, Amsterdam.

Barnes, H. A., Hutton, J. F., and Walters, K. (1989b). *An introduction to rheology*, chapter 2. Elsevier, Amsterdam.

Batten, S., Champness, N., Chen, X.-M., Garcia-Martinez, J., Kitagawa, S., Öhrström, L., O'Keeffe, M., Suh, M., and Reedijk, J. (2013). Terminology of metal-organic frameworks and coordination polymers (IUPAC recommendations 2013). *Pure and Applied Chemistry*, 85(8):1715–1724.

Beamson, G. and Briggs, D. (1992). *High resolution XPS of organic polymers : the Scienta ESCA300 database*. Wiley.

Bendrea, A.-D., Cianga, L., and Cianga, I. (2011). Review paper: Progress in the field of conducting polymers for tissue engineering applications. *Journal of Biomaterials Applications*, 26(1):3–84.

Bergenstråhle, M., Wohlert, J., Himmel, M., and Brady, J. (2010). Simulation studies of the insolubility of cellulose. *Carbohydrate Research*, 345(14):2060–2066.

Bird, R., Stewart, W., and Lightfoot, E. (2007). *Transport phenomena*, chapter 1. J. Wiley, New York.

Blachot, J.-F., Brunet, N., Navard, P., and Cavaillé, J.-Y. (1998). Rheological behavior of cellulose/monohydrate of n-methylmorpholine n-oxide solutions part 1: Liquid state. *Rheologica Acta*, 37:107–114.

Blackwell, J. (2012). About the structure of cellulose: debating the lindman hypothesis. *Cellulose*, 19(3):594.

Bétard, A. and Fischer, R. (2012). Metal-organic framework thin films: From fundamentals to applications. *Chemical Reviews*, 112(2):1055–1083.

Carlsson, D., Nyström, G., Zhou, Q., Berglund, L., Nyholm, L., and Stromme, M. (2012). Electroactive nanofibrillated cellulose aerogel composites with tunable structural and electrochemical properties. *Journal of Materials Chemistry*, 22(36):19014–19024.

Centrone, A., Yang, Y., Speakman, S., Bromberg, L., Rutledge, G. C., and Hatton, T. A. (2010). Growth of metal-organic frameworks on polymer surfaces. *Journal of the American Chemical Society*, 132(44):15687–15691.

Chen, W., Weng, S., Zhang, F., Allen, S., Li, X., Bao, L., Lam, R. H. W., Macoska, J. A., Merajver, S. D., and Fu, J. (2013). Nanoroughened surfaces for efficient capture of circulating tumor cells without using capture antibodies. *ACS Nano*, 7(1):566–575.

Chronakis, I. S., Grapenson, S., and Jakob, A. (2006). Conductive polypyrrole nanofibers via electrospinning: Electrical and morphological properties. *Polymer*, 47(5):1597–1603.

Chui, S. S.-Y., Lo, S. M.-F., Charmant, J. P. H., Orpen, A. G., and Williams, I. D. (1999). A chemically functionalizable nanoporous material $[Cu_3(TMA)_2(H_2O)_3]n$. *Science*, 283(5405):1148–1150.

Cooper, A., Bhattarai, N., and Zhang, M. (2011). Fabrication and cellular compatibility of aligned chitosan-PCL fibers for nerve tissue regeneration. *Carbohydrate Polymers*, 85(1):149–156.

Cross, M. (1965). Rheology of non-newtonian fluids: A new flow equation for pseudoplastic systems. *Journal of Colloid Science*, 20(5):417–437.

Czaja, A., Trukhan, N., and Müller, U. (2009). Industrial applications of metal-organic frameworks. *Chemical Society Reviews*, 38(5):1284–1293.

da Silva Pinto, M., Sierra-Avila, C., and Hinestroza, J. (2012). In situ synthesis of a Cu-BTC metal-organic framework (MOF 199) onto cellulosic fibrous substrates: Cotton. *Cellulose*, 19(5):1771–1779.

De Vrieze, S., Van Camp, T., Nelvig, A., Hagström, B., Westbroek, P., and De Clerck, K. (2009). The effect of temperature and humidity on electrospinning. *Journal of Materials Science*, 44(5):1357–1362.

Dumas, J. B., Brogniart, A., and Pelonze, T. J. (1839). Rapport sur un mémoire de M. Payen, relatif à là composition de la matière ligneuse. *Comptes Rendus*, 8:51–53.

Earle, M. and Seddon, K. (2000). Ionic liquids. green solvents for the future. *Pure and Applied Chemistry*, 72(7):1391–1398.

Ebner, G., Schiehser, S., Potthast, A., and Rosenau, T. (2008). Side reaction of cellulose with common 1-alkyl-3-methylimidazolium-based ionic liquids. *Tetrahedron Letters*, 49(51):7322 – 7324.

Fink, H.-P., Hofmann, D., and Philipp, B. (1995). Some aspects of lateral chain order in cellulosics from x-ray scattering. *Cellulose*, 2(1):51–70.

Fonner, J. M., Forciniti, L., Nguyen, H., Byrne, J. D., Kou, Y.-F., Syeda-Nawaz, J., and Schmidt, C. E. (2008). Biocompatibility implications of polypyrrole synthesis techniques. *Biomedical Materials*, 3(3):034124.

Formhals, A. (1934). Process and apparatus for preparing artificial threads. U.S. Patent 1,975,504, U.S. Patent and Trademark Office.

Freire, M., Teles, A., Ferreira, R., Carlos, L., Lopes-Da-Silva, J., and Coutinho, J. (2011). Electrospun nanosized cellulose fibers using ionic liquids at room temperature. *Green Chemistry*, 13(11):3173–3180.

French, A., Miller, D., and Aabloo, A. (1993). Miniature crystal models of cellulose polymorphs and other carbohydrates. *International Journal of Biological Macromolecules*, 15(1):30–36.

Férey, G., Serre, C., Devic, T., Maurin, G., Jobic, H., Llewellyn, P., De Weireld, G., Vimont, A., Daturi, M., and Chang, J.-S. (2011). Why hybrid porous solids capture greenhouse gases? *Chemical Society Reviews*, 40(2):550–562.

Frey, M. (2008). Electrospinning cellulose and cellulose derivatives. *Polymer Reviews*, 48(2):378–391.

Gardner, K. H. and Blackwell, J. (1974). The structure of native cellulose. *Biopolymers*, 13(10):1975–2001.

Gliemann, H. and Wöll, C. (2012). Epitaxially grown metal-organic frameworks. *Materials Today*, 15(3):110 – 116.

Graenacher, C. (1934). Cellulose solution. U.S. Patent 1,943,176, U.S. Patent and Trademark Office.

Greiner, A. and Wendorff, J. H. (2007). Electrospinning: A fascinating method for the preparation of ultrathin fibers. *Angewandte Chemie International Edition*, 46(30):5670–5703.

Guimard, N., Gomez, N., and Schmidt, C. (2007). Conducting polymers in biomedical engineering. *Progress in Polymer Science (Oxford)*, 32(8-9):876–921.

Hasani, M. (2010). *Chemical modification of cellulose-new possibilities of some classical routes*. PhD dissertation, Chalmers University of Technology.

Hauru, L., Hummel, M., King, A., Kilpeläinen, I., and Sixta, H. (2012). Role of solvent parameters in the regeneration of cellulose from ionic liquid solutions. *Biomacromolecules*, 13(9):2896–2905.

Haworth, W. N. and Machemer, H. (1932). Molecular structure of cellulose. *J. Chem. Soc.*, pages 2270–2277.

He, X., Xiao, Q., Lu, C., Wang, Y., Zhang, X., Zhao, J., Zhang, W., Zhang, X., and Deng, Y. (2014). Uniaxially aligned electrospun all-cellulose nanocomposite nanofibers reinforced with cellulose nanocrystals: Scaffold for tissue engineering. *Biomacromolecules*, 15(2):618–627.

Henriksson, M., Berglund, L. A., Isaksson, P., Lindström, T., and Nishino, T. (2008). Cellulose nanopaper structures of high toughness. *Biomacromolecules*, 9(6):1579–1585.

Henriksson, M., Henriksson, G., Berglund, L., and Lindström, T. (2007). An environmen-

tally friendly method for enzyme-assisted preparation of microfibrillated cellulose (MFC) nanofibers. *European Polymer Journal*, 43(8):3434 – 3441.

Öhrström, L. and Larsson, K. (2005). *Molecule-Based Materials, The Structural Network Approach*. Elsevier.

Irvine, J. C. and Hirst, E. L. (1923). The molecular structure of cotton cellulose. *J. Chem. Soc., Trans.*, 123:518–532.

Jia, B., Li, Y., Yang, B., Xiao, D., Zhang, S., Rajulu, A., Kondo, T., Zhang, L., and Zhou, J. (2013). Effect of microcrystal cellulose and cellulose whisker on biocompatibility of cellulose-based electrospun scaffolds. *Cellulose*, 20(4):1911–1923.

Jin, R., Bian, Z., Li, J., Ding, M., and Gao, L. (2013). ZIF-8 crystal coatings on a polyimide substrate and their catalytic behaviours for the knoevenagel reaction. *Dalton Transactions*, 42:3936–3940.

Kaynak, A. and Beltran, R. (2003). Effect of synthesis parameters on the electrical conductivity of polypyrrole-coated poly(ethylene terephthalate) fabrics. *Polymer International*, 52(6):1021–1026.

Khanjani, S. and Morsali, A. (2014). Ultrasound-promoted coating of MOF-5 on silk fiber and study of adsorptive removal and recovery of hazardous anionic dye "congo red". *Ultrasonics Sonochemistry*, 21(4):1424–1429.

Köhler, S., Liebert, T., Schöbitz, M., Schaller, J., Meister, F., Günther, W., and Heinze, T. (2007). Interactions of ionic liquids with polysaccharides 1. unexpected acetylation of cellulose with 1-ethyl-3-methylimidazolium acetate. *Macromolecular Rapid Communications*, 28(24):2311–2317.

Kida, K., Okita, M., Fujita, K., Tanaka, S., and Miyake, Y. (2013). Formation of high crystalline ZIF-8 in an aqueous solution. *CrystEngComm*, 15(9):1794–1801.

Kim, C.-W., Frey, M., Marquez, M., and Joo, Y. (2005). Preparation of submicron-scale, electrospun cellulose fibers via direct dissolution. *Journal of Polymer Science, Part B: Polymer Physics*, 43(13):1673–1683.

Kondo, T. (2004). *Polysaccharides Structural Diversity and Functional Versatility, Second Edition*, chapter 3. CRC Press.

Kosan, B., Michels, C., and Meister, F. (2008). Dissolution and forming of cellulose with ionic liquids. *Cellulose*, 15(1):59–66.

Kreno, L., Leong, K., Farha, O., Allendorf, M., Van Duyne, R., and Hupp, J. (2012). Metal-organic framework materials as chemical sensors. *Chemical Reviews*, 112(2):1105–1125.

Küsgens, P., Siegle, S., and Kaskel, S. (2009). Crystal growth of the metal-organic framework $Cu_3(BTC)_2$ on the surface of pulp fibers. *Advanced Engineering Materials*, 11(1-2):93–95.

Kuzmenko, V., Naboka, O., Gatenholm, P., and Enoksson, P. (2014). Ammonium chloride promoted synthesis of carbon nanofibers from electrospun cellulose acetate. *Carbon*, 67:694 – 703.

Laine, J., Lindström, T., Nordmark, G., and Risinger, G. (2000). Studies on topochemical modification of cellulosic fibres. part 1. chemical conditions for the attachment of carboxymethyl cellulose onto fibres. *Nordic Pulp and Paper Research Journal*, 15(5):520–526.

Lange, L. E. and Obendorf, S. K. (2015). Functionalization of cotton fiber by partial etherification and self-assembly of polyoxometalate encapsulated in $Cu_3(BTC)_2$ metal-organic framework. *ACS Applied Materials & Interfaces*, 7(7):3974–3980.

Lee, J. Y., Bashur, C. A., Goldstein, A. S., and Schmidt, C. E. (2009). Polypyrrole-coated electrospun PLGA nanofibers for neural tissue applications. *Biomaterials*, 30(26):4325 – 4335.

Li, D. and Xia, Y. (2004). Electrospinning of nanofibers: Reinventing the wheel? *Advanced Materials*, 16(14):1151–1170.

Li, Y. and Yang, R. (2008). Hydrogen storage in metal-organic and covalent-organic frameworks by spillover. *AIChE Journal*, 54(1):269–279.

Lian, Z., Huimin, L., and Zhaofei, O. (2014). In situ crystal growth of zeolitic imidazolate frameworks (ZIF) on electrospun polyurethane nanofibers. *Dalton Transactions*, 43:6684–6688.

Liu, C., Hsu, P.-C., Lee, H.-W., Ye, M., Zheng, G., Liu, N., Li, W., and Cui, Y. (2015). Transparent air filter for high-efficiency pm 2.5 capture. *Nature Communications*, 6(6205).

Liu, H. and Hsieh, Y.-L. (2002). Ultrafine fibrous cellulose membranes from electrospinning of cellulose acetate. *Journal of Polymer Science Part B: Polymer Physics*, 40(18):2119–2129.

Liu, X., Gilmore, K. J., Moulton, S. E., and Wallace, G. G. (2009). Electrical stimulation

promotes nerve cell differentiation on polypyrrole/poly (2-methoxy-5 aniline sulfonic acid) composites. *Journal of Neural Engineering*, 6(6):065002.

Ma, Z., Kotaki, M., and Ramakrishna, S. (2005). Electrospun cellulose nanofiber as affinity membrane. *Journal of Membrane Science*, 265:115–123.

Malarkey, E. B., Fisher, K. A., Bekyarova, E., Liu, W., Haddon, R. C., and Parpura, V. (2009). Conductive single-walled carbon nanotube substrates modulate neuronal growth. *Nano Letters*, 9(1):264–268.

Medronho, B., Romano, A., Miguel, M., Stigsson, L., and Lindman, B. (2012). Rationalizing cellulose (in)solubility: reviewing basic physicochemical aspects and role of hydrophobic interactions. *Cellulose*, 19(3):581–587.

Morris, W., Stevens, C. J., Taylor, R. E., Dybowski, C., Yaghi, O. M., and Garcia-Garibay, M. A. (2012). Nmr and x-ray study revealing the rigidity of zeolitic imidazolate frameworks. *The Journal of Physical Chemistry C*, 116(24):13307–13312.

Mueller, U., Schubert, M., Teich, F., Puetter, H., Schierle-Arndt, K., and Pastré, J. (2006). Metal-organic frameworks - prospective industrial applications. *Journal of Materials Chemistry*, 16(7):626–636.

Nishino, T., Takano, K., and Nakamae, K. (1995). Elastic modulus of the crystalline regions of cellulose polymorphs. *Journal of Polymer Science Part B: Polymer Physics*, 33(11):1647–1651.

Nyström, G., Mihranyan, A., Razaq, A., Lindström, T., Nyholm, L., and Strømme, M. (2010). A nanocellulose polypyrrole composite based on microfibrillated cellulose from wood. *Journal of Physical Chemistry B*, 114(12):4178–4182.

O' Sullivan, A. (1997). Cellulose: the structure slowly unravels. *Cellulose*, 4:173–207.

Okita, Y., Saito, T., and Isogai, A. (2010). Entire surface oxidation of various cellulose microfibrils by tempo-mediated oxidation. *Biomacromolecules*, 11(6):1696–1700.

Olsson, C., Hedlund, A., Idström, A., and Westman, G. (2014). Effect of methylimidazole on cellulose/ionic liquid solutions and regenerated material therefrom. *Journal of Materials Science*, 49(9):3423–3433.

Ostermann, R., Cravillon, J., Weidmann, C., Wiebcke, M., and Smarsly, B. (2011). Metal-organic framework nanofibers via electrospinning. *Chemical Communications*, 47(1):442–444.

Ott, E., Spurlin, H. M., and Grafflin, M. W. (1954). *Cellulose and Cellulose Derivatives*, chapter I. Interscience Publishers, Inc, New York, second edition.

Ozer, R. R. and Hinestroza, J. P. (2015). One-step growth of isoreticular luminescent metal-organic frameworks on cotton fibers. *RSC Adv.*, 5:15198–15204.

Pan, Y., Liu, Y., Zeng, G., Zhao, L., and Lai, Z. (2011). Rapid synthesis of zeolitic imidazolate framework-8 (ZIF-8) nanocrystals in an aqueous system. *Chemical Communications*, 47(7):2071–2073.

Park, K., Ni, Z., Côté, A., Choi, J., Huang, R., Uribe-Romo, F., Chae, H., O'Keeffe, M., and Yaghi, O. (2006). Exceptional chemical and thermal stability of zeolitic imidazolate frameworks. *Proceedings of the National Academy of Sciences of the United States of America*, 103(27):10186–10191.

Payen, A. (1838). Mémoire sur la composition du tissu propre des plantes et du ligneux. *Comptes Rendus*, 7:1052–1056.

Pham, T. P. T., Cho, C.-W., and Yun, Y.-S. (2010). Environmental fate and toxicity of ionic liquids: A review. *Water Research*, 44(2):352 – 372.

Pimentel, B., Parulkar, A., Zhou, E.-K., Brunelli, N., and Lively, R. (2014). Zeolitic imidazolate frameworks: Next-generation materials for energy-efficient gas separations. *ChemSusChem*, 7(12):3202–3240.

Prabhakaran, M., Venugopal, J., Chyan, T., Hai, L., Chan, C., Lim, A., and Ramakrishna, S. (2008). Electrospun biocomposite nanofibrous scaffolds for neural tissue engineering. *Tissue Engineering - Part A.*, 14(11):1787–1797.

Quan, S.-L., Kang, S.-G., and Chin, I.-J. (2010). Characterization of cellulose fibers electrospun using ionic liquid. *Cellulose*, 17(2):223–230.

Ramakrishna, S., Fujihara, K., Teo, W.-E., Yong, T., Ma, Z., and Ramaseshan, R. (2006). Electrospun nanofibers: Solving global issues. *Materials Today*, 9(3):40–50.

Ranby, B. G. (1951). Fibrous macromolecular systems. cellulose and muscle. the colloidal properties of cellulose micelles. *Discuss. Faraday Soc.*, 11:158–164.

Razaq, A., Nyholm, L., Sjödin, M., Strømme, M., and Mihranyan, A. (2012). Paper-based energy-storage devices comprising carbon fiber-reinforced polypyrrole-cladophora nanocellulose composite electrodes. *Advanced Energy Materials*, 2(4):445–454.

Revol, J.-F., Bradford, H., Giasson, J., Marchessault, R., and Gray, D. (1992). Helicoidal self-ordering of cellulose microfibrils in aqueous suspension. *International Journal of Biological Macromolecules*, 14(3):170–172.

Rodríguez, H. S., Hinestroza, J. P., Ochoa-Puentes, C., Sierra, C. A., and Soto, C. Y. (2014a). Antibacterial activity against escherichia coli of Cu−BTC (MOF-199) metal-organic framework immobilized onto cellulosic fibers. *Journal of Applied Polymer Science*, 131(19).

Rodríguez, K., Renneckar, S., and Gatenholm, P. (2011). Biomimetic calcium phosphate crystal mineralization on electrospun cellulose-based scaffolds. *ACS Applied Materials and Interfaces*, 3(3):681–689.

Rodríguez, K., Sundberg, J., Gatenholm, P., and Renneckar, S. (2014b). Electrospun nanofibrous cellulose scaffolds with controlled microarchitecture. *Carbohydrate Polymers*, 100:143–149.

Rogers, R. D. and Seddon, K. R. (2003). Ionic liquids–solvents of the future? *Science*, 302(5646):792–793.

Rose, M., Böhringer, B., Jolly, M., Fischer, R., and Kaskel, S. (2011). MOF processing by electrospinning for functional textiles. *Advanced Engineering Materials*, 13(4):356–360.

Rosseinsky, M. J., Smith, M. W., and Timperley, C. M. (2015). Metal-organic frameworks: Breaking bad chemicals down. *Nature Materials*, 14(5):469–470.

Saito, T., Nishiyama, Y., Putaux, J.-L., Vignon, M., and Isogai, A. (2006). Homogeneous suspensions of individualized microfibrils from tempo-catalyzed oxidation of native cellulose. *Biomacromolecules*, 7(6):1687–1691.

Schmidt, C., Shastri, V., Vacanti, J., and Langer, R. (1997). Stimulation of neurite outgrowth using an electrically conducting polymer. *Proceedings of the National Academy of Sciences of the United States of America*, 94(17):8948–8953.

Schwanninger, M., Rodrigues, J., Pereira, H., and Hinterstoisser, B. (2004). Effects of short-time vibratory ball milling on the shape of FT-IR spectra of wood and cellulose. *Vibrational Spectroscopy*, 36(1):23 – 40.

Shekhah, O., Wang, H., Kowarik, S., Schreiber, F., Paulus, M., Tolan, M., Sternemann, C., Evers, F., Zacher, D., Fischer, R., and Wöll, C. (2007). Step-by-step route for the synthesis of metal-organic frameworks. *Journal of the American Chemical Society*, 129(49):15118–15119.

Sheldon, R. (2005). Green solvents for sustainable organic synthesis: State of the art. *Green Chemistry*, 7(5):267–278.

Staudinger, H. (1920). Über polymerisation. *Berichte der deutschen chemischen Gesellschaft (A and B Series)*, 53(6):1073–1085.

Staudinger, H. and Fritschi, J. (1922). Über isopren und kautschuk. 5. mitteilung. Über die hydrierung des kautschuks und über seine konstitution. *Helvetica Chimica Acta*, 5(5):785–806.

Subbiah, T., Bhat, G. S., Tock, R. W., Parameswaran, S., and Ramkumar, S. S. (2005). Electrospinning of nanofibers. *Journal of Applied Polymer Science*, 96(2):557–569.

Sui, X., Yuan, J., Yuan, W., and Zhou, M. (2008). Preparation of cellulose nanofibers/nanoparticles via electrospray. *Chemistry Letters*, 37(1):114–115.

Swatloski, R., Spear, S., Holbrey, J., and Rogers, R. (2002). Dissolution of cellose with ionic liquids. *Journal of the American Chemical Society*, 124(18):4974–4975.

Talin, A., Centrone, A., Ford, A., Foster, M., Stavila, V., Haney, P., Kinney, R., Szalai, V., El Gabaly, F., Yoon, H., Léonard, F., and Allendorf, M. (2014). Tunable electrical conductivity in metal-organic framework thin-film devices. *Science*, 343(6166):66–69.

Tanaka, S., Kida, K., Okita, M., Ito, Y., and Miyake, Y. (2012). Size-controlled synthesis of zeolitic imidazolate framework-8 (ZIF-8) crystals in an aqueous system at room temperature. *Chemistry Letters*, 41(10):1337–1339.

Taylor, G. (1964). Disintegration of Water Drops in an Electric Field. *Royal Society of London Proceedings Series A*, 280:383–397.

Turbak, A. F., Snyder, F. W., and Sandberg, K. R. (1983). Suspensions containing microfibrillated cellulose. U.S. Patent 4378381, U.S. Patent and Trademark Office.

Viswanathan, G., Murugesan, S., Pushparaj, V., Nalamasu, O., Ajayan, P. M., and Linhardt, R. J. (2006). Preparation of biopolymer fibers by electrospinning from room temperature ionic liquids. *Biomacromolecules*, 7(2):415–418.

Wang, Z., Tammela, P., Zhang, P., Strømme, M., and Nyholm, L. (2014). Efficient high active mass paper-based energy-storage devices containing free-standing additive-less polypyrrole-nanocellulose electrodes. *Journal of Materials Chemistry A*, 2(21):7711–7716.

Warwicker, J. O. and Wright, A. C. (1967). Function of sheets of cellulose chains in swelling reactions on cellulose. *Journal of Applied Polymer Science*, 11(5):659–671.

Woodings, C. (2001). *Regenerated cellulose fibres*, chapter 1. A brief history of regenerated cellulosic fibres. Woodhead Publishing Ltd.

Wu, X.-F., Salkovskiy, Y., and Dzenis, Y. A. (2011). Modeling of solvent evaporation from polymer jets in electrospinning. *Applied Physics Letters*, 98(22).

Wu, Y.-N., Li, F., Liu, H., Zhu, W., Teng, M., Jiang, Y., Li, W., Xu, D., He, D., Hannam, P., and Li, G. (2012). Electrospun fibrous mats as skeletons to produce free-standing MOF membranes. *Journal of Materials Chemistry*, 22(33):16971–16978.

Xu, S., Zhang, J., He, A., Li, J., Zhang, H., and Han, C. (2008). Electrospinning of native cellulose from nonvolatile solvent system. *Polymer*, 49(12):2911–2917.

Yakovenko, A., Reibenspies, J., Bhuvanesh, N., and Zhou, H.-C. (2013). Generation and applications of structure envelopes for porous metal-organic frameworks. *Journal of Applied Crystallography*, 46(2):346–353.

Yamane, C., Aoyagi, T., Ago, M., Sato, K., Okajima, K., and Takahashi, T. (2006). Two different surface properties of regenerated cellulose due to structural anisotropy. *Polymer Journal*, 38(8):819–826.

Zacher, D., Shekhah, O., Wöll, C., and Fischer, R. (2009). Thin films of metal-organic frameworks. *Chemical Society Reviews*, 38(5):1418–1429.

Zeleny, J. (1917). Instability of electrified liquid surfaces. *Phys. Rev.*, 10:1–6.